Addressing the R D (■) anomalies with an S 1 leptoquark fAddressing the R D (■) anomalies with an S 1 leptoquark from SO(10) grand unificationrom SO(10) grand unification

by

Ufuk Aydemir, Tanumoy Mandal, Subhadip Mitra

in

Physics review D

Report No: IIIT/TR/2020/-1

Centre for Computational Natural Sciences and Bioinformatics
International Institute of Information Technology
Hyderabad - 500 032, INDIA
January 2020

Addressing the $R_{D^{(*)}}$ anomalies with an S_1 leptoquark from SO(10) grand unification

Ufuk Aydemir,[1,2,*] Tanumoy Mandal,[3,4,†] and Subhadip Mitra[5,‡]

[1]*Institute of High Energy Physics, Chinese Academy of Sciences, Beijing 100049, P. R. China*
[2]*School of Physics, Huazhong University of Science and Technology, Wuhan, Hubei 430074, P. R. China*
[3]*Department of Physics and Astronomy, Uppsala University, Box 516, SE-751 20 Uppsala, Sweden*
[4]*Department of Physics and Astrophysics, University of Delhi, Delhi 110 007, India*
[5]*Center for Computational Natural Sciences and Bioinformatics, International Institute of Information Technology, Hyderabad 500 032, India*

(Received 4 September 2019; published 22 January 2020)

Motivated by the $R_{D^{(*)}}$ anomalies, we investigate an SO(10) grand unification scenario where a charge $-1/3$ scalar leptoquark (S_1) remains as the only new physics candidate at the TeV scale. This leptoquark along with the Standard Model (SM) Higgs doublet originates from the same ten-dimensional real scalar multiplet in the SO(10) grand unification framework taking its mass close to the electroweak scale. We explicitly show how the gauge coupling unification is achieved with only one intermediate symmetry-breaking scale at which the Pati-Salam gauge group is broken into the SM group. We investigate the phenomenological implications of our scenario and show that an S_1 with a specific Yukawa texture can explain the $R_{D^{(*)}}$ anomalies. We perform a multiparameter scan considering the relevant flavor constraints on $R_{D^{(*)}}$, $F_L(D^*)$, $P_\tau(D^*)$ and $R^{\nu\nu}_{K^{(*)}}$ as well as the constraint coming from the $Z \to \tau\tau$ decay and the latest $\tau\tau$ resonance search data at the LHC. Our analysis shows that a single leptoquark solution to the observed $R_{D^{(*)}}$ anomalies with S_1 is still a viable solution.

DOI: 10.1103/PhysRevD.101.015011

I. INTRODUCTION

During the past few years, several disagreements between experiments and the Standard Model (SM) predictions in the rare B decays have been reported by the *BABAR* [1,2], LHCb [3–7] and Belle [8–11] collaborations. So far, these anomalies have been quite persistent. The most significant ones have been observed in the $R_{D^{(*)}}$ and $R_{K^{(*)}}$ observables, defined as,

$$R_{D^{(*)}} = \frac{\mathrm{BR}(B \to D^{(*)}\tau\nu)}{\mathrm{BR}(B \to D^{(*)}\ell\nu)} \quad \text{and}$$
$$R_{K^{(*)}} = \frac{\mathrm{BR}(B \to K^{(*)}\mu^+\mu^-)}{\mathrm{BR}(B \to K^{(*)}e^+e^-)}.$$

Here, $\ell = \{e \text{ or } \mu\}$ and BR stands for branching ratio. The experimental values of R_D and R_{D^*} are in excess of their SM predictions [12–15] by 1.4σ and 2.5σ, respectively, (combined excess of 3.08σ in $R_{D^{(*)}}$) based on the world averages as of spring 2019, according to the Heavy Flavor Averaging Group [16], whereas, the observed R_K and R_{K^*} are both suppressed compared to their SM predictions [17,18] by $\sim 2.6\sigma$.

One of the possible explanations for the B-decay anomalies is the existence of scalar leptoquarks whose masses are in the few-TeV range [19–53]).[1] Leptoquarks, which posses both lepton and quark couplings, often exist in the grand unified theories (GUTs) or in the Pati-Salam-type models. Considering that the LHC searches, except for these anomalies, have so far returned empty handed, if the leptoquarks indeed turn out to be behind these anomalies, it is likely that there will only be a small number of particles to be discovered. However, their existence in small numbers at the TeV scale would be curious in terms of its implications regarding physics beyond the Standard Model. Scalars in these models mostly come in large multiplets and it would be peculiar that only one or a few of the components become light at the TeV scale while others remain heavy. Mass splitting is actually a well-speculated subject in the literature in the context of the infamous doublet-triplet splitting problem in supersymmetric theories and GUTs. From this point of view, even the SM Higgs

*uaydemir@ihep.ac.cn
†tanumoy.mandal@physics.uu.se
‡subhadip.mitra@iiit.ac.in

Published by the American Physical Society under the terms of the Creative Commons Attribution 4.0 International license. Further distribution of this work must maintain attribution to the author(s) and the published article's title, journal citation, and DOI. Funded by SCOAP³.

[1]See Refs. [54–61] for the vector-leptoquark solutions proposed to explain the B-decay anomalies.

in a GUT framework is troublesome if it turns out to be the only scalar at the electroweak (EW) scale.

In this paper, we consider a single scalar leptoquark, $S_1(3,1,-1/3)$, at the TeV scale, in the SO(10) GUT framework [62–75]. This particular leptoquark was discussed in the literature to be responsible for one (or possibly both) of the $R_{D^{(*)}}$ and $R_{K^{(*)}}$ anomalies [21,22,25,32]. (Later, however, it was shown in Ref. [45] that a single S_1 leptoquark can only alleviate the $R_{K^{(*)}}$ discrepancy, but cannot fully resolve it.) Furthermore, it is contained in a relatively small multiplet that resides in the fundamental representation of the SO(10) group, a real **10**, together with a scalar doublet with the quantum numbers that allow it to be identified as the SM Higgs. Therefore, S_1 being the only light scalar entity other than the SM Higgs doublet is justified in this scenario. A future discovery of such a leptoquark at the TeV scale could be interpreted as evidence in favor of an SO(10) GUT.

It has been argued in the literature that a real $\mathbf{10}_H$ in the minimal SO(10) setup (even together with a real $\mathbf{120}_H$ or a complex $\mathbf{120}_H$) is not favored in terms of a realistic Yukawa sector [68]. On the other hand, it has been recently discussed in Ref. [75] that a Yukawa sector consisting of a real $\mathbf{10}_H$, a real $\mathbf{120}_H$ and a complex $\mathbf{126}_H$, can establish a realistic Yukawa sector due to the contributions from the scalars whose quantum numbers are the same as the SM Higgs doublet. Thus, this is the scalar content we assign in our model for the Yukawa sector.

The inclusion of S_1 in the particle content of the model at the TeV scale does not improve the status of the SM in terms of gauge coupling unification, which cannot be realized by the particle content in question. Fortunately, in the SO(10) framework, there are other ways to unify the gauge coupling constants, in contrast to models based on the SU(5) group which also contains such a leptoquark within the same multiplet as the SM Higgs. As we illustrate in this paper, inserting a single intermediate phase where the active gauge group is the Pati-Salam group, $\mathrm{SU}(4)_C \otimes \mathrm{SU}(2)_L \otimes \mathrm{SU}(2)_R$, which appears to be the favored route of symmetry breaking by various phenomenological bounds [71], establishes coupling unification as desired. In our model, the Pati-Salam group is broken into the SM gauge group at an intermediate energy scale M_C, while SO(10) is broken into the Pati-Salam group at the unification scale M_U. We consider two versions of this scenario, depending on whether the left-right symmetry, so-called D parity, is broken together with SO(10) at M_U, or it is broken at a later stage, at M_C, where the Pati-Salam symmetry is broken into the SM gauge symmetry.

Light color triplets, similar to the one we consider in this paper, are often dismissed for the sake of proton stability since these particles in general have the right quantum numbers for them to couple potentially dangerous operators that mediate proton decay. On the other hand, the proton stability could possibly be ensured through various symmetry mechanisms such as the utilization of Peccei-Quinn (PQ) symmetry [68,76], other U(1) symmetries such as the one discussed in Ref. [77], or a discrete symmetry similar to the one considered in Ref. [22]. Operators leading to proton decay could also be suppressed by a specific mechanism such as the one discussed in Ref. [78] or they could be completely forbidden by geometrical reasons [38]. In this paper, we adopt a discrete symmetry as suggested in Ref. [22], assumed to operate below the intermediate symmetry-breaking scale even though it is not manifest at higher energies.

Motivated by the possible existence of a single TeV-scale S_1 in the SO(10) GUT framework, we move on to investigate the phenomenological implications of our model. In Ref. [22], it was shown that a TeV-scale S_1 leptoquark can explain the $R_{D^{(*)}}$ anomalies while simultaneously inducing the desired suppression in $R_{K^{(*)}}$ through box diagrams. Since the most significant anomalies are seen in the $R_{D^{(*)}}$ observables, in this paper, we concentrate mostly on scenarios that can accommodate these observables. Generally, a TeV-scale S_1 requires one Yukawa coupling to be large to accommodate the $R_{D^{(*)}}$ anomalies [32,45]. This, however, could create a problem for the $b \to s\bar{\nu}\nu$ transition rate measured in the $R_K^{\nu\nu}$ observable. In the SM, this decay proceeds through a loop whereas S_1 can contribute at the tree level in this transition. Therefore, the measurement of $R_K^{\nu\nu}$ is very important to restrict the parameter space of S_1.[2] Some specific Yukawa couplings of S_1 are also severely constrained from the $Z \to \tau\tau$ decay [47] and the LHC $\tau\tau$ resonance search data [48]. Therefore, it is evident that in order to find the $R_{D^{(*)}}$-favored parameter space while successfully accommodating other relevant constraints, one has to introduce new d.o.f. in terms of new couplings and/or new particles. Here, we consider a specific Yukawa texture with three free couplings to show that a TeV-scale S_1, consistent with relevant measurements, can still explain the $R_{D^{(*)}}$ anomalies.

The rest of the paper is organized as follows. In Sec. II, we introduce our model. In Sec. III, we display the unification of the couplings for two versions of our model. In Sec. IV, we present the related LHC phenomenology with a single extra leptoquark S_1. We display the exclusion limits from the LHC data and discuss related future prospects. We also study the renormalization group (RG) running of the Yukawa couplings. Finally in Sec. V, we end our paper with a discussion and conclusions.

II. THE SO(10) MODEL

In our SO(10) model, we entertain the idea that the SM Higgs doublet is not the only scalar multiplet at the TeV

[2]One can avoid this conflict by introducing some additional degrees of freedom (d.o.f.), as shown in Ref. [30]. There, the authors introduced an S_3 leptoquark in addition to the S_1 to concomitantly explain $R_{D^{(*)}}$ and $R_{K^{(*)}}$ while being consistent with $R_K^{\nu\nu}$.

scale, but it is accompanied by a leptoquark $S_1 = (3, 1, -1/3)$, both of which reside in a real ten-dimensional representation, **10**, of SO(10) group. The peculiar mass splitting among the components of this multiplet does not occur, leading to a naturally light scalar leptoquark at the TeV scale.

We start with a real $\mathbf{10}_H$ of SO(10) whose Pati-Salam and SM decompositions are given as

$$\begin{aligned}\mathbf{10} &= (1,2,2)_{422} \oplus (6,1,1)_{422} \\ &= \underbrace{\left(1,2,\frac{1}{2}\right)_{321}}_{H} \oplus \underbrace{\left(1,2,-\frac{1}{2}\right)_{321}}_{H^*} \oplus \underbrace{\left(3,1,-\frac{1}{3}\right)_{321}}_{S_1} \\ &\quad \oplus \underbrace{\left(\bar{3},1,\frac{1}{3}\right)_{321}}_{S_1^*},\end{aligned} \tag{1}$$

where subscripts denote the corresponding gauge group and we set $Q = I_3 + Y$.

The scalar content we assign for the Yukawa sector consists of a real $\mathbf{10}_H$, a real $\mathbf{120}_H$, and a complex $\mathbf{126}_H$, which establishes a realistic Yukawa sector through mixing between the scalars whose quantum numbers are the same as the SM Higgs doublet, as shown in Ref. [75]. Note that

$$\mathbf{16} \otimes \mathbf{16} = \mathbf{10}_s \oplus \mathbf{120}_a \oplus \mathbf{126}_s, \tag{2}$$

where **16** is the spinor representation in which each family of fermions, including the right-handed neutrino, resides in. The subscripts s and a denote the symmetric and antisymmetric components. The Pati-Salam decompositions of **120** and **126** are given as

$$\begin{aligned}\mathbf{120} &= (1,2,2)_{422} \oplus (1,1,10)_{422} \oplus (1,1,\overline{10})_{422} \\ &\quad \oplus (6,3,1)_{422} \oplus (6,1,3)_{422} \oplus (15,2,2)_{422}, \\ \mathbf{126} &= (10,3,1)_{422} \oplus (\overline{10},1,3)_{422} \oplus (15,2,2)_{422} \\ &\quad \oplus (6,1,1)_{422}.\end{aligned} \tag{3}$$

The Yukawa terms are then given as

$$\mathcal{L}_Y = \mathbf{16}_F(Y_{10}\mathbf{10}_H + Y_{120}\mathbf{120}_H + Y_{126}\overline{\mathbf{126}}_H)\mathbf{16}_F + \text{H.c.}, \tag{4}$$

where Y_{10} and Y_{126} are complex Yukawa matrices, symmetric in the generation space, and Y_{120} is a complex antisymmetric one.

The SM doublet contained in $\phi(1,2,2)_{422}$ of **10** is mixed with other doublets accommodated in $\phi(1,2,2)_{422}$ and $\Sigma(15,2,2)_{422}$ of the real multiplet **120** and $\Sigma(15,2,2)_{422}$ of **126**, yielding a Yukawa sector consistent with the observed fermion masses [75]. The fermion mass matrices for the up quark, down quark, charged leptons, Dirac neutrinos and Majorana neutrinos are given as [75]

$$\begin{aligned}M_U &= v_{10}Y_{10} + v_{126}^u Y_{126} + (v_{120}^{(1)} + v_{120}^{(15)})Y_{120}, \\ M_D &= v_{10}Y_{10} + v_{126}^d Y_{126} + (v_{120}^{(1)} + v_{120}^{(15)})Y_{120}, \\ M_E &= v_{10}Y_{10} - 3v_{126}^d Y_{126} + (v_{120}^{(1)} - 3v_{120}^{(15)})Y_{120}, \\ M_{\nu_D} &= v_{10}Y_{10} - 3v_{126}^u Y_{126} + (v_{120}^{(1)} - 3v_{120}^{(15)})Y_{120}, \\ M_{\nu_{R,L}} &= v_{R,L}Y_{126},\end{aligned} \tag{5}$$

where $v_i^u(v_i^d)$ are the presumed vacuum expectation values of the neutral components of the corresponding bidoublets, contributing to the masses of the up quarks and the Dirac neutrinos (the down quarks and the charged leptons), and where

$$\begin{aligned}v_{10} &\equiv v_{10}^u = v_{10}^d, \\ v_{120}^{(1)} &\equiv v_{120}^{u,(1)} = v_{120}^{d,(1)}, \\ v_{120}^{(15)} &\equiv v_{120}^{u,(15)} = v_{120}^{d,(15)},\end{aligned} \tag{6}$$

due to the reality condition of **10** and **120**. The superscripts (1) and (15) denote the doublets residing in $\phi(1,2,2)_{422}$ and $\Sigma(15,2,2)_{422}$ of **120**, respectively. v_R in the Majorana mass matrices given in Eq. (5) is the vacuum expectation value of the SM singlet contained in $(\overline{10},1,3)_{422}$ and is responsible for the heavy masses of the right-handed neutrinos (type-I seesaw), and $v_L \sim v_R v_{10}^2/M_{GUT}^2$ is induced by the potential term $\mathbf{10}_H^2\mathbf{120}_H^2$ and is responsible for the left-handed Majorana neutrino masses (type-II seesaw) [75].

For the symmetry-breaking pattern, we consider a scenario in which the intermediate phase has the gauge symmetry of the Pati-Salam group $\mathrm{SU}(4)_C \otimes \mathrm{SU}(2)_L \otimes \mathrm{SU}(2)_R$. Note that this specific route of symmetry breaking appears to be favored by various phenomenological bounds [71]. We consider two versions of this scenario depending on whether or not the Pati-Salam gauge symmetry is accompanied by the D-parity invariance, a $\mathbb{Z}_2$ symmetry that maintains the complete equivalence of the left and right sectors [65,66,79], after the SO(10) breaking. The symmetry-breaking sequence is schematically given as

$$\mathrm{SO}(10) \xrightarrow[\langle\mathbf{210}\rangle\,(\text{or}\,\langle\mathbf{54}\rangle)]{M_U} G_{422\,(\text{or}\,422D)} \xrightarrow[\langle\mathbf{126}\rangle]{M_C} G_{321}(\mathrm{SM}) \xrightarrow[\langle\mathbf{10}\rangle]{M_Z} G_{31}, \tag{7}$$

where, we use the notation,

$$\begin{aligned}G_{422D} &\equiv \mathrm{SU}(4)_C \otimes \mathrm{SU}(2)_L \otimes \mathrm{SU}(2)_R \otimes D, \\ G_{422} &\equiv \mathrm{SU}(4)_C \otimes \mathrm{SU}(2)_L \otimes \mathrm{SU}(2)_R, \\ G_{321} &\equiv \mathrm{SU}(3)_C \otimes \mathrm{SU}(2)_L \otimes \mathrm{U}(1)_Y, \\ G_{31} &\equiv \mathrm{SU}(3)_C \otimes \mathrm{U}(1)_Q.\end{aligned} \tag{8}$$

The first stage of the spontaneous symmetry breaking occurs through the Pati-Salam singlet in the SO(10) multiplet **210**, acquiring a vacuum expectation value (VEV) at the unification scale M_U. This singlet is odd under D parity and, therefore, the resulting symmetry group is G_{422} in the first stage of the symmetry breaking. In the second step, the breaking of G_{422} into the SM gauge group G_{321} is realized through the SM singlet contained in $\Delta_R(\overline{10},1,3)_{422}$ of **126**, acquiring a VEV at the energy scale M_C, which also yields a Majorana mass for the right-handed neutrino. The last stage of the symmetry breaking is realized predominantly through the SM doublet contained in $\phi(1,2,2)_{422}$ of **10**. The mass scale of these Pati-Salam multiplets is set as M_C, the energy scale at which the Pati-Salam symmetry is broken into the SM, while the rest of the fields are assumed to be heavy at the unification scale M_U. The only d.o.f., assumed to survive down to the electroweak scale, are the SM Higgs doublet and the color triplet, S_1. We call this model A_1.

In the second scenario, which we call model A_2, the first stage of the symmetry breaking is realized through the Pati-Salam singlet contained in **54**, which acquires a VEV. This singlet is even under D parity, and therefore, D parity is not broken at this stage with the SO(10) symmetry, and the resulting symmetry group valid down to M_C is G_{422}. The rest of the symmetry breaking continues in the same way as in model A_1. Consequently in model A_2, we include one more Pati-Salam multiplet at M_C, $\Delta_L(10,3,1)$, in order to maintain a complete left-right symmetry down to M_C. The scalar content and, for later use, the corresponding RG coefficients in each energy interval are given in Table I.

Finally, the relevant Lagrangian for phenomenological analysis at low energy is given by

$$\mathcal{L} \supset (D_\mu S_1)^\dagger (D^\mu S_1) - M_{S_1}^2 |S_1|^2 - \lambda |S_1|^2 |H|^2 + (\mathbf{\Lambda}^L \bar{Q}^c i\tau_2 L + \mathbf{\Lambda}^R \bar{u}_R^c e_R) S_1^\dagger + \text{H.c.} \tag{9}$$

where Q and L are the SM quark and lepton doublets (for each family), $\mathbf{\Lambda}^{L/R}$ are coupling matrices in flavor space and $\psi^c = C\bar{\psi}^T$ are charge-conjugate spinors. Notice the absence of dangerous diquark couplings of S_1 that would lead to proton decay. One way to forbid these couplings is to impose a $\mathbb{Z}_2$ symmetry [22] that emerges below the Pati-Salam breaking scale under which quarks and leptons transform with opposite parities whereas the leptoquark is assigned odd parity, i.e., $(q, l, S_1) \to (\pm q, \mp l, -S_1)$. Note also that the inclusion of S_1 can affect the stability of the electroweak vacuum via loop effects. The relevant discussion can be found in Ref. [80].

Evidently, the Lagrangian given in Eq. (9) together with the SM Lagrangian should be understood in the effective field theory context. The new and SM Yukawa couplings in the TeV-scale Lagrangian are induced from the original SO(10) Yukawa couplings each of which is generated by a linear combination of unification-scale operators and gets modified due to the mixing effects induced by the scalar fields that have Yukawa couplings to three chiral families of $\mathbf{16}_F$. It is indeed this rich structure that enables the realization of a fermion mass spectrum consistent with the expected fermion masses of the SM model at the unification scale, as shown in Ref. [75]. As we will discuss later in Sec. IV G, the modification to the SM RG running of the Yukawa couplings due to the inclusion of $\mathbf{\Lambda}^{L/R}$ does not register strong changes in the fermionic mass spectrum and hence the main message of Ref. [75] is valid in our case, as well.

III. GAUGE COUPLING UNIFICATION

In this section, after we lay out the preliminaries for one-loop RG running and show that the new particle content at the TeV scale does not lead to the unification of the SM gauge couplings directly, we illustrate gauge coupling unification with a single intermediate step of symmetry breaking. Once the particle content at low energies is determined, there may be numerous ways to unify the gauge couplings, depending on the selection of the scalar content in SO(10) representations. In the literature, the canonical way to make this selection is through adopting a minimalistic approach, allowed by the observational constraints. In the following, we pursue the same strategy while taking into account the analysis made in Ref. [75] for a realistic Yukawa sector.

A. One-loop RG running

For a given particle content, the gauge couplings in an energy interval $[M_A, M_B]$ evolve under one-loop RG running as

TABLE I. The scalar content and the RG coefficients in the energy intervals for model $A_{1,2}$. Note that the ϕ fields, the Φ field, and one of the Σ fields originate from real SO(10) multiplets and thus the $\eta = 1/2$ condition should be employed when necessary while determining the RG coefficients in Eq. (11).

Interval	Scalar content for model A_1 (A_2)	RG coefficients
II	$\phi(1,2,2)\times 2$, $\Phi(6,1,1)$, $\Sigma(15,2,2)\times 2$, $\Delta_R(\overline{10},1,3)$, (and $\Delta_L(10,3,1)$ for model A_2)	$[a_4, a_L, a_R] = [\frac{1}{2}(\frac{7}{2}), \frac{9}{2}(\frac{67}{6}), \frac{67}{6}]$
I	$H(1,2,\frac{1}{2})$, $S_1(3,1,-\frac{1}{3})$	$[a_3, a_2, a_1] = [\frac{-41}{6}, \frac{-19}{6}, \frac{125}{18}]$

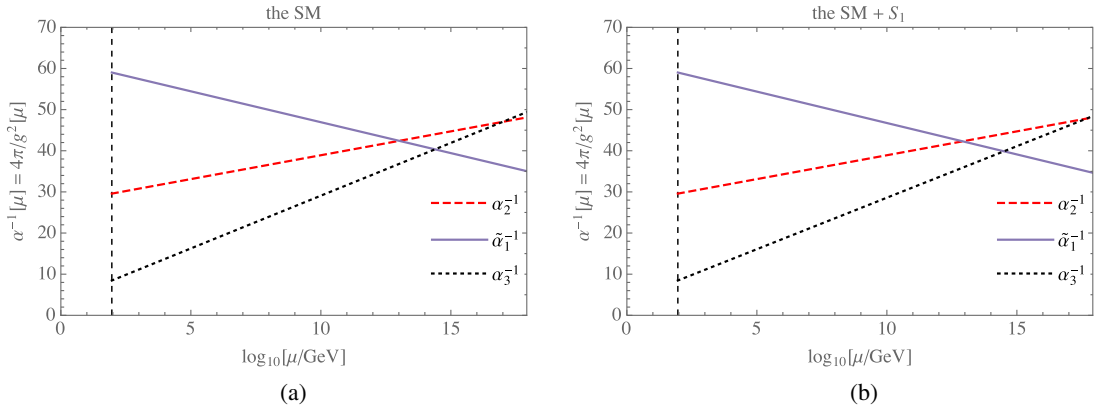

FIG. 1. Running of the gauge couplings with the particle content of the SM and with the inclusion of S_1. The vertical dotted line corresponds to the electroweak scale M_Z. For α_1^{-1}, we plot the redefined quantity $\tilde{\alpha}_1^{-1} \equiv \frac{3}{5}\alpha_1^{-1}$ as required by the SO(10) boundary conditions. Including the leptoquark in the particle content does not provide a significant modification to the SM RG running in favor of unification.

$$\frac{1}{g_i^2(M_A)} - \frac{1}{g_i^2(M_B)} = \frac{a_i}{8\pi^2}\ln\frac{M_B}{M_A}, \tag{10}$$

where the RG coefficients a_i are given by [81,82]

$$a_i = -\frac{11}{3}C_2(G_i) + \frac{2}{3}\sum_{R_f} T_i(R_f)\cdot d_1(R_f)\cdots d_n(R_f) + \frac{\eta}{3}\sum_{R_s} T_i(R_s)\cdot d_1(R_s)\cdots d_n(R_s), \tag{11}$$

and the full gauge group is given as $G = G_i \otimes G_1 \otimes \ldots \otimes G_n$. The summation in Eq. (11) is over irreducible chiral representations of fermions (R_f) and irreducible representations of scalars (R_s) in the second and third terms, respectively. The coefficient η is either 1 or 1/2, depending on whether the corresponding representation is complex or (pseudo)real, respectively. $d_j(R)$ is the dimension of the representation R under the group $G_{j\neq i}$. $C_2(G_i)$ is the quadratic Casimir for the adjoint representation of the group G_i, and T_i is the Dynkin index of each representation (see Table II). For the U(1) group, $C_2(G) = 0$ and

TABLE II. Dynkin index T_i for various irreducible representations of SU(2), SU(3), and SU(4). Our normalization convention in this paper follows the one adopted in Ref. [82]. Notice that there are two inequivalent 15-dimensional irreducible representations for SU(3).

Representation	SU(2)	SU(3)	SU(4)
2	$\frac{1}{2}$	–	–
3	2	$\frac{1}{2}$	–
4	5	–	$\frac{1}{2}$
6	$\frac{35}{2}$	$\frac{5}{2}$	1
8	42	3	–
10	$\frac{165}{2}$	$\frac{15}{2}$	3
15	280	$10, \frac{35}{2}$	4

$$\sum_{f,s} T = \sum_{f,s} Y^2, \tag{12}$$

where Y is the $\mathrm{U}(1)_Y$ charge.

The addition of S_1 to the particle content of the SM does not help in unifying the gauge couplings as displayed in Fig. 1, where the RG running is performed with the modified RG coefficients given in Table I in interval I, while interval II is irrelevant to this particular case. Unification of the gauge couplings can be established through intermediate symmetry breaking between the electroweak scale and unification scale, as we illustrate in the next subsection with a single intermediate step of symmetry breaking.

B. Unification with a single intermediate scale

We start by labeling the energy intervals in between symmetry-breaking scales $[M_Z, M_C]$ and $[M_C, M_U]$ with Roman numerals as

$$\begin{aligned} &\mathrm{I}\colon [M_Z, M_C], \quad G_{213}(\mathrm{SM}), \\ &\mathrm{II}\colon [M_C, M_U], \quad G_{224} \quad \text{or} \quad G_{224D}. \end{aligned} \tag{13}$$

The boundary/matching conditions we impose on the couplings at the symmetry-breaking scales are

$$\begin{aligned} &M_U\colon\ g_L(M_U) = g_R(M_U) = g_4(M_U), \\ &M_C\colon\ g_3(M_C) = g_4(M_C), \qquad g_2(M_C) = g_L(M_C), \\ &\frac{1}{g_1^2(M_C)} = \frac{1}{g_R^2(M_C)} + \frac{2}{3}\frac{1}{g_4^2(M_C)}, \\ &g_L(M_C) = g_R(M_C)\ \text{(absent in the } G_{224}\text{ case)}, \\ &M_Z\colon\ \frac{1}{e^2(M_Z)} = \frac{1}{g_1^2(M_Z)} + \frac{1}{g_2^2(M_Z)}. \end{aligned} \tag{14}$$

TABLE III. The predictions of models A_1 and A_2.

Model	A_1	A_2
$\log_{10}(M_U/\mathrm{GeV})$	17.1	15.6
$\log_{10}(M_C/\mathrm{GeV})$	10.9	13.7
α_U^{-1}	29.6	35.4

We use the central values of the low-energy data as the boundary conditions in the RG running (in the $\overline{\mathrm{MS}}$ scheme) [83,84]: $\alpha^{-1} = 127.95$, $\alpha_s = 0.118$, $\sin^2\theta_W = 0.2312$ at $M_Z = 91.2$ GeV, which translate to $g_1 = 0.357$, $g_2 = 0.652$, $g_3 = 1.219$. The coupling constants are all required to remain in the perturbative regime during the evolution from M_Z to M_U.

The RG coefficients, a_i, differ depending on the particle content in each energy interval, changing every time symmetry breaking occurs. Together with the matching and boundary conditions, one-loop RG running leads to the following conditions on the symmetry-breaking scales M_U and M_C:

$$2\pi\left[\frac{3-8\sin^2\theta_W(M_Z)}{\alpha(M_Z)}\right] = (3a_1 - 5a_2)\ln\frac{M_C}{M_Z} + (-5a_L + 3a_R + 2a_4)\ln\frac{M_U}{M_C},$$
$$2\pi\left[\frac{3}{\alpha(M_Z)} - \frac{8}{\alpha_s(M_Z)}\right] = (3a_1 + 3a_2 - 8a_3)\ln\frac{M_C}{M_Z} + (3a_L + 3a_R - 6a_4)\ln\frac{M_U}{M_C}, \tag{15}$$

where the notation on a_i is self-evident. The unified gauge coupling α_U at the scale M_U is then obtained from

$$\frac{2\pi}{\alpha_U} = \frac{2\pi}{\alpha_s(M_Z)} - \left(a_4\ln\frac{M_U}{M_C} + a_3\ln\frac{M_C}{M_Z}\right). \tag{16}$$

Thus, once the RG coefficients in each interval are specified, the scales M_U and M_C, and the value of α_U are uniquely determined. The results are given in Table III, and unification of the couplings is displayed in Fig. 2 for each model.

As mentioned previously, we assume in this paper that the proton-decay-mediating couplings of S_1 are suppressed. On the other hand, we do not make any assumptions regarding the other potentially dangerous operators which could lead to proton decay. Thus, it is necessary to inspect whether the predictions of our models displayed in Table III are compatible with the current bounds coming from the proton decay searches or not. The most recent and stringent bound on the lifetime of the proton comes from the mode $p \to e^+\pi^0$, and is $\tau_p > 1.6\times 10^{34}$ years [85]. As for the proton decay modes that are mediated by the super-heavy gauge bosons, which reside in the adjoint representation of SO(10) **45**, considering that $\tau_p \sim M_U^4/m_p^5\alpha_U^2$ [86], we obtain $M_U \gtrsim 10^{15.9}$ GeV, which is consistent with predictions of both model A_1 and model A_2, within an order of magnitude of the latter. Additionally, since M_C is the scale at which the Pati-Salam symmetry breaks into the SM, it determines the expected mass values for the proton-decay-mediating color triplets. From a naive analysis [71], it can be shown that the current bounds on the proton lifetime require $M_C \gtrsim 10^{11}$ GeV, again consistent with the predictions of both model A_1 and model A_2, within an order of magnitude of the former. Note that these bounds should be taken as order-of-magnitude estimates since, while obtaining them, we approximate the anticipated masses of the super-heavy gauge bosons and the color triplets as $M_X \approx M_U$ and $M_T \approx M_C$, while it would not be unreasonable to expect that these mass values could differ from the corresponding energy scales within an order of magnitude.

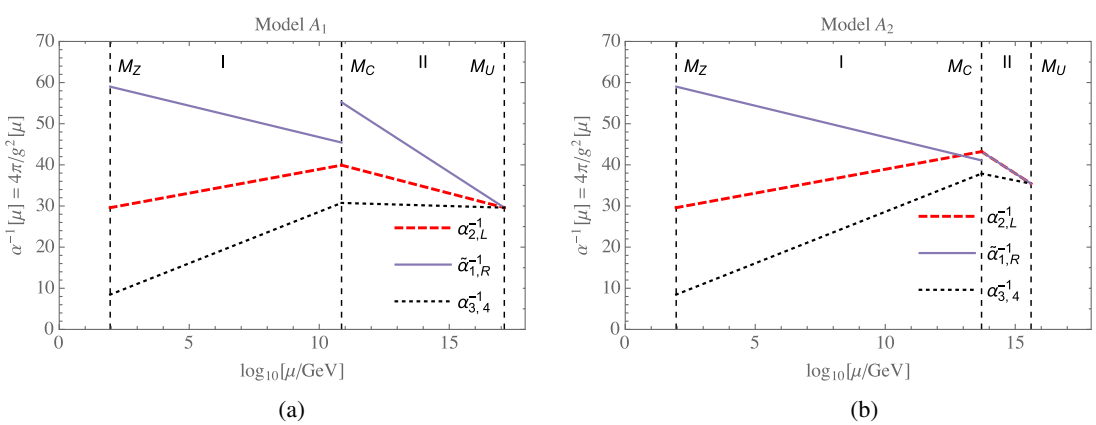

FIG. 2. Running of the gauge couplings for models A_1 and A_2. Note that $\tilde{\alpha}_1^{-1} \equiv \frac{3}{5}\alpha_1^{-1}$. The discontinuity at M_C in each plot is due to the boundary conditions given in Eq. (14).

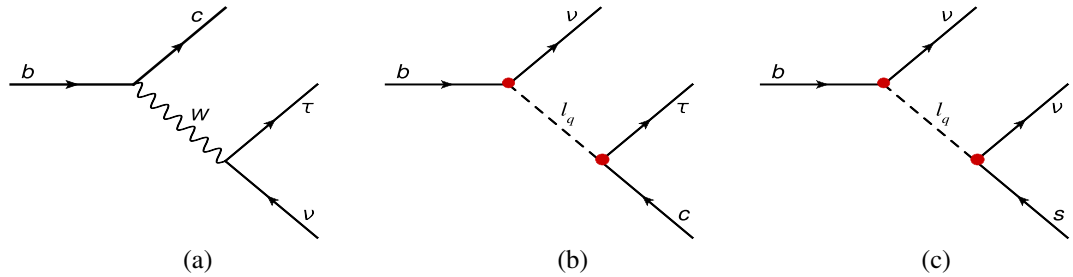

FIG. 3. Leading-order parton-level Feynman diagrams responsible for the $B \to D^{(*)}\tau\nu$ decay (a) in the SM, and (b) in the S_1 model. The parton-level process in the presence of S_1 that would contribute to $B \to K\nu\nu$ is shown in diagram (c).

IV. LOW-ENERGY PHENOMENOLOGY

The existence of a TeV-scale charge $-1/3$ scalar leptoquark in a GUT framework is quite interesting from a phenomenological perspective mainly for two reasons. First, its existence is testable at the LHC. The direct-detection searches for scalar leptoquarks have been putting exclusion bounds on S_1 with different decay hypotheses [87,88]. Second, as mentioned earlier, such a leptoquark can offer an explanation of some persistent flavor anomalies observed in several experiments. For example, if we consider the anomalies observed in the B-meson semileptonic decays via charged currents (collectively these show the most significant departure from the SM expectations), S_1 can provide an explanation if it couples with τ and neutrino(s) and b and c quarks. The direct LHC bounds on such a leptoquark are not very severe but as it has been pointed out in Ref. [48], the present LHC data in the $pp \to \tau\tau/\tau\nu$ channels have actually put constraints on the S_1 parameter space relevant for explaining the observed $R_{D^{(*)}}$ anomalies. Here, using flavor data and LHC constraints, we obtain the allowed parameter space in our model. We also point out some possible new search channels at the LHC. On the flavor side, our primary focus is on the charged-current anomalies observed in the semileptonic B decays in the $R_{D^{(*)}}$ observables. Hence, as in Ref. [48], we focus on the interaction terms of S_1 that could play a role to address the $R_{D^{(*)}}$ anomalies for simplicity.

A. The S_1 model

The single TeV-scale S_1 leptoquark that originates from the GUT model discussed in Sec. II transforms under the SM gauge group as $(3, 1, -1/3)$. The low-energy interactions of S_1 with the SM fields are shown in a compact manner in Eq. (9). Below, we display the relevant interaction terms required for our phenomenological analysis,

$$\mathcal{L} \supset [\lambda^L_{ij}\bar{Q}^c_i(i\tau_2)L_j + \lambda^R_{ij}\bar{u}^c_i\ell_{Rj}]S_1^\dagger + \text{H.c.}, \qquad (17)$$

where Q_i and L_i denote the ith-generation quark and lepton doublets, respectively and λ^H_{ij} represents the coupling of S_1 with a charge-conjugate quark of the ith generation and a lepton of the jth generation with chirality H. Without any loss of generality, we assume all λ's are real in our collider analysis since the LHC data that we consider are insensitive to their complex nature. Also, we only consider mixing among quarks [Cabibbo-Kobayashi-Maskawa (CKM) mixing] and ignore neutrino mixing (Pontecorvo-Maki-Nakagawa-Sakata mixing) completely as all neutrino flavors contribute to the missing energy and hence are not distinguishable at the LHC. The couplings of S_1 to the first-generation SM fermions are heavily constrained [32]. Hence, we assume $\lambda_{1i}, \lambda_{i1} = 0$ in our analysis.[3]

The parton-level Feynman diagrams for the $b \to c\tau\nu$ decay (responsible for the $B \to D^{(*)}\tau\nu$ decay) are shown in Fig. 3. In order to have a nonzero contribution in the $R_{D^{(*)}}$ observables from S_1, we need the $b\nu S_1$ and $c\tau S_1$ couplings to be nonzero simultaneously. Minimally, one can start with just a single free coupling: either λ^L_{23} or λ^L_{33}. The coupling λ^L_{23} (λ^L_{33}) directly generates the $c\tau S_1$ ($b\nu S_1$) interaction and the other one, i.e., the $b\nu S_1$ ($c\tau S_1$) can be generated through the CKM mixing among quarks. These two minimal scenarios were discussed in detail in Ref. [48]. For these two cases, the Lagrangian in Eq. (17) can be written explicitly as,

$$C_1:\ \mathcal{L} \supset \lambda^L_{23}[\bar{c}^c\tau_L - (V_{cb}\bar{b}^c + V_{cs}\bar{s}^c + V_{cd}\bar{d}^c)\nu]S_1^\dagger + \text{H.c.} \quad (\lambda^L_{33} = 0), \qquad (18)$$

$$C_2:\ \mathcal{L} \supset \lambda^L_{33}[(V^*_{ub}\bar{u}^c + V^*_{cb}\bar{c}^c + V^*_{tb}\bar{t}^c)\tau_L - \bar{b}^c\nu]S_1^\dagger + \text{H.c.} \quad (\lambda^L_{23} = 0). \qquad (19)$$

In Ref. [48], it was shown that for C_1, the $R_{D^{(*)}}$-favored parameter space is already ruled out by the latest LHC data. On the other hand, C_2 is not seriously constrained by the LHC data since this scenario is insensitive to the coupling λ^L_{33}. Only the pair-production searches, which are largely

[3]However, these couplings can be generated through the CKM mixing. We refer the interested readers to Ref. [32] for various important flavor constraints in this regard.

insensitive to λ_{33}^L, in the $tt\tau\tau$ and $bb\nu\nu$ modes exclude M_{S_1} up to 900 GeV [87] and 1100 GeV [88], respectively for a 100% BR in each decay mode. However, Ref. [47] showed that the $R_{D^{(*)}}$-favored parameter space in C_2 is also ruled out by the electroweak precision data on the $Z \to \tau\tau$ decay.

The above two minimal cases, C_1 and C_2, are the two extremes. One can, however, consider a next-to-minimal situation, where both λ_{23}^L and λ_{33}^L are nonzero to explain $R_{D^{(*)}}$ anomalies being within the LHC bounds [48]. However, $B \to K^{(*)}\nu\nu$ decay results severely constrain such a scenario due to the tree-level leptoquark contribution [see Fig. 3(c)]. References [32,45] indicated that a large λ_{23}^R might help explain various flavor anomalies simultaneously while being consistent with other relevant experimental results.

In this paper, we allow λ_{23}^L, λ_{33}^L and λ_{23}^R to be nonzero and perform a parameter scan for a single S_1 solution of the $R_{D^{(*)}}$ anomalies. We locate the $R_{D^{(*)}}$-favored parameter space that satisfies the limits from $B \to K^{(*)}\nu\nu$ and $Z \to \tau\tau$ decays and is still allowed by the latest LHC data. A S_1 can also provide new final states at the LHC like $\tau\tau + \text{jets}$ and $\tau + \not{E}_T + \text{jets}$ in which leptoquarks have not been searched for before.

B. $R_{D^{(*)}}$ with S_1

In the SM, the semitauonic B decay is mediated by the left-handed charged currents and the corresponding four-Fermi interactions are given by the following effective Lagrangian:

$$\mathcal{L}_{\rm SM} = -\frac{4G_F}{\sqrt{2}} V_{cb}[\bar{c}\gamma^\mu P_L b][\bar{\tau}\gamma_\mu P_L \nu_\tau]. \tag{20}$$

In the presence of new physics, there are a total of five four-Fermi operators that appear in the effective Lagrangian for the $B \to D^{(*)}\tau\nu$ decay [89],

$$\mathcal{L} \supset -\frac{4G_F}{\sqrt{2}} V_{cb}[(1+\mathcal{C}_{V_L})\mathcal{O}_{V_L} + \mathcal{C}_{V_R}\mathcal{O}_{V_R} + \mathcal{C}_{S_L}\mathcal{O}_{S_R} + \mathcal{C}_{S_R}\mathcal{O}_{S_R} + \mathcal{C}_{T_R}\mathcal{O}_{T_R}], \tag{21}$$

where the $\mathcal{C}_X$'s are the Wilson coefficients associated with the effective operators:

(1) Vector operators:

$$\mathcal{O}_{V_L} = [\bar{c}\gamma^\mu P_L b][\bar{\tau}\gamma_\mu P_L \nu],$$
$$\mathcal{O}_{V_R} = [\bar{c}\gamma^\mu P_R b][\bar{\tau}\gamma_\mu P_L \nu].$$

(2) Scalar operators:

$$\mathcal{O}_{S_L} = [\bar{c}P_L b][\bar{\tau}P_L \nu],$$
$$\mathcal{O}_{S_R} = [\bar{c}P_R b][\bar{\tau}P_L \nu].$$

(3) Tensor operator:

$$\mathcal{O}_{T_L} = [\bar{c}\sigma^{\mu\nu}P_L b][\bar{\tau}\sigma_{\mu\nu}P_L \nu].$$

The operator $\mathcal{O}_{V_L}$ is SM-like and the other four operators introduce new Lorentz structures into the Lagrangian. Note that the operator $\mathcal{O}_{T_R}$ is identically zero, i.e.,

$$\mathcal{O}_{T_R} = [\bar{c}\sigma^{\mu\nu}P_R b][\bar{\tau}\sigma_{\mu\nu}P_L \nu] = 0. \tag{22}$$

The S_1 leptoquark that we consider can generate only $\mathcal{O}_{V_L,S_L,T_L}$. Hence, the coefficients of the other two operators, namely, $\mathcal{C}_{V_R}$ and $\mathcal{C}_{S_R}$ remain zero in our model. In terms of the S_1 parameters the Wilson coefficients can be expressed as,

$$\left.\begin{aligned} \mathcal{C}_{V_L} &= \frac{1}{2\sqrt{2}G_F V_{cb}} \frac{\lambda_{23}^{L*}\lambda_{33}^L}{2M_{S_1}^2}, \\ \mathcal{C}_{S_L} &= -\frac{1}{2\sqrt{2}G_F V_{cb}} \frac{\lambda_{33}^L\lambda_{23}^R}{2M_{S_1}^2}, \\ \mathcal{C}_{T_L} &= -\frac{1}{4}\mathcal{C}_{S_L}. \end{aligned}\right\} \tag{23}$$

These relations are obtained at the mass scale M_{S_1}. However, running of the strong coupling constant down to $m_b \sim 4.2$ GeV changes these coefficients substantially except for $\mathcal{C}_{V_L}$ which is protected by the QCD Ward identity. As a result, the ratio $\mathcal{C}_{S_L}/\mathcal{C}_{T_L}$ becomes,

$$\left.\frac{\mathcal{C}_{S_L}}{\mathcal{C}_{T_L}}\right|_{m_b} = \rho(m_b, M_{S_1})\left.\frac{\mathcal{C}_{S_L}}{\mathcal{C}_{T_L}}\right|_{M_{S_1}} = -4\rho(m_b, M_{S_1}). \tag{24}$$

The modification factor ρ can be obtained from Ref. [32], and we display it in Fig. 4. In terms of the nonzero Wilson coefficients we can express the ratios $r_{D^{(*)}} = R_{D^{(*)}}/R_{D^{(*)}}^{\rm SM}$ as [49],

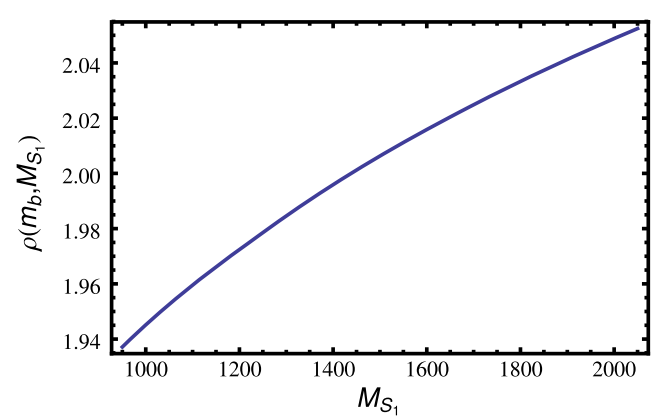

FIG. 4. The ratio defined in Eq. (24), $\rho(m_b, M_{S_1}) = \frac{\mathcal{C}_{S_L}}{\mathcal{C}_{T_L}}(\mu = m_b)/\frac{\mathcal{C}_{S_L}}{\mathcal{C}_{T_L}}(\mu = M_{S_1})$, obtained from Ref. [32].

TABLE IV. Summary of the $R_{D^{(*)}}$ related inputs for our parameter scan.

Observable	Experimental average	SM expectation	Ratio	Value
R_D	$0.340 \pm 0.027 \pm 0.013$ [16]	0.299 ± 0.003 [12]	r_D	1.137 ± 0.101
R_{D^*}	$0.295 \pm 0.011 \pm 0.008$ [16]	0.258 ± 0.005 [16]	r_{D^*}	1.144 ± 0.057
$F_L(D^*)$	$0.60 \pm 0.08 \pm 0.035$ [10,11]	0.46 ± 0.04 [92]	$f_L(D^*)$	1.313 ± 0.198
$P_\tau(D^*)$	$-0.38 \pm 0.51^{+0.21}_{-0.16}$ [90]	-0.497 ± 0.013 [89]	$p_\tau(D^*)$	0.766 ± 1.093

$$r_D \equiv \frac{R_D}{R_D^{\rm SM}} \approx |1+\mathcal{C}_{V_L}|^2 + 1.02|\mathcal{C}_{S_L}|^2 + 0.9|\mathcal{C}_{T_L}|^2 + 1.49{\rm Re}[(1+\mathcal{C}_{V_L})\mathcal{C}_{S_L}^*] + 1.14{\rm Re}[(1+\mathcal{C}_{V_L})\mathcal{C}_{T_L}^*], \tag{25}$$

$$r_{D^*} \equiv \frac{R_{D^*}}{R_D^{\rm SM}} \approx |1+\mathcal{C}_{V_L}|^2 + 0.04|\mathcal{C}_{S_L}|^2 + 16.07|\mathcal{C}_{T_L}|^2 - 0.11\,{\rm Re}[(1+\mathcal{C}_{V_L})\mathcal{C}_{S_L}^*] - 5.12\,{\rm Re}[(1+\mathcal{C}_{V_L})\mathcal{C}_{T_L}^*]. \tag{26}$$

With Eq. (24) one can simplify the above equations as,

$$r_D = |1+\mathcal{C}_{V_L}|^2 + \left(1.02 + \frac{0.9}{16\rho^2}\right)|\mathcal{C}_{S_L}|^2 + \left(1.49 - \frac{1.14}{4\rho}\right){\rm Re}[(1+\mathcal{C}_{V_L})\mathcal{C}_{S_L}^*], \tag{27}$$

$$r_{D^*} = |1+\mathcal{C}_{V_L}|^2 + \left(0.04 + \frac{16.07}{16\rho^2}\right)|\mathcal{C}_{S_L}|^2 - \left(0.11 - \frac{5.12}{4\rho}\right){\rm Re}[(1+\mathcal{C}_{V_L})\mathcal{C}_{S_L}^*], \tag{28}$$

where $\rho = \rho(m_b, M_{S_1})$. There are two other observables related to the R_{D^*}—the longitudinal D^* polarization $F_L(D^*)$ and the longitudinal τ polarization asymmetry $P_\tau(D^*)$—which have recently been measured by the Belle Collaboration [10,11,90]. In terms of the nonzero Wilson coefficients in our model, $F_L(D^*)$ and $P_\tau(D^*)$ are expressed as [49],

$$f_L(D^*) \equiv \frac{F_L(D^*)}{F_L^{\rm SM}(D^*)} \approx \frac{1}{r_{D^*}}\{|1+\mathcal{C}_{V_L}|^2 + 0.08|\mathcal{C}_{S_L}|^2 + 7.02|\mathcal{C}_{T_L}|^2 - 0.24\,{\rm Re}[(1+\mathcal{C}_{V_L})\mathcal{C}_{S_L}^*] - 4.37\,{\rm Re}[(1+\mathcal{C}_{V_L})\mathcal{C}_{T_L}^*]\}, \tag{29}$$

$$p_\tau(D^*) \equiv \frac{P_\tau(D^*)}{P_\tau^{\rm SM}(D^*)} \approx \frac{1}{r_{D^*}}\{|1+\mathcal{C}_{V_L}|^2 - 0.07|\mathcal{C}_{S_L}|^2 - 1.86\times|\mathcal{C}_{T_L}|^2 + 0.22\,{\rm Re}[(1+\mathcal{C}_{V_L})\mathcal{C}_{S_L}^*] - 3.37\,{\rm Re}[(1+\mathcal{C}_{V_L})\mathcal{C}_{T_L}^*]\}. \tag{30}$$

These equations can further be simplified as,

$$f_L(D^*) = \frac{1}{r_{D^*}}\left\{|1+\mathcal{C}_{V_L}|^2 + \left(0.08 + \frac{7.02}{16\rho^2}\right)|\mathcal{C}_{S_L}|^2 - \left(0.24 - \frac{4.37}{4\rho}\right){\rm Re}[(1+\mathcal{C}_{V_L})\mathcal{C}_{S_L}^*]\right\}, \tag{31}$$

$$p_\tau(D^*) = \frac{1}{r_{D^*}}\left\{|1+\mathcal{C}_{V_L}|^2 - \left(0.07 + \frac{1.86}{16\rho^2}\right)|\mathcal{C}_{S_L}|^2 + \left(0.22 + \frac{3.37}{4\rho}\right){\rm Re}[(1+\mathcal{C}_{V_L})\mathcal{C}_{S_L}^*]\right\}. \tag{32}$$

These two observables have the power to discriminate between new physics models with different Lorentz structures (see e.g., Ref. [91]). In Table IV, we list the bounds on the $R_{D^{(*)}}$ related observables that we include in our parameter scan.

C. Constraint from $R^{\nu\nu}_{K^{(*)}}$

The SM flavor-changing neutral-current $b \to s\bar{\nu}\nu$ transition proceeds through a loop and is suppressed by the Glashow-Iliopoulos-Maiani mechanism, whereas in our model, S_1 can mediate this transition at the tree level [see Fig. 3(c)]. Therefore, this neutral-current decay can heavily constrain the parameter space of our model. We define the following ratio:

$$R^{\nu\nu}_{K^{(*)}} = \frac{\Gamma(B \to K^{(*)}\nu\nu)}{\Gamma(B \to K^{(*)}\nu\nu)_{\rm SM}}. \tag{33}$$

The current experimental 90% confidence limit (C.L.) upper limits on the above quantities are $R^{\nu\nu}_K < 3.9$ and $R^{\nu\nu}_{K^*} < 2.7$ [93]. In terms of our model parameters, $R^{\nu\nu}_{K^{(*)}}$ is given by the following expression:

$$R^{\nu\nu}_{K^{(*)}} = 1 - \frac{2a}{3M_{S_1}^2}{\rm Re}\left(\frac{\lambda_{23}^{L*}\lambda_{33}^L}{V_{tb}V_{ts}^*}\right) + \frac{a^2}{3M_{S_1}^4}\left|\frac{\lambda_{23}^{L*}\lambda_{33}^L}{V_{tb}V_{ts}^*}\right|^2, \tag{34}$$

where $a = \sqrt{2}\pi^2/(e^2 G_F |C_L^{\rm SM}|)$ with $C_L^{\rm SM} \approx -6.38$ [32]. We use this constraint in our analysis and find that it significantly restricts our parameter space. Note that this constraint applies on λ_{23}^L and λ_{33}^L but not on λ_{23}^R. In Fig. 5, we show the regions in the $\lambda_{23}^L - \lambda_{33}^L$ plane with $R^{\nu\nu}_{K^*} < 2.7$ for two different values of M_{S_1}.

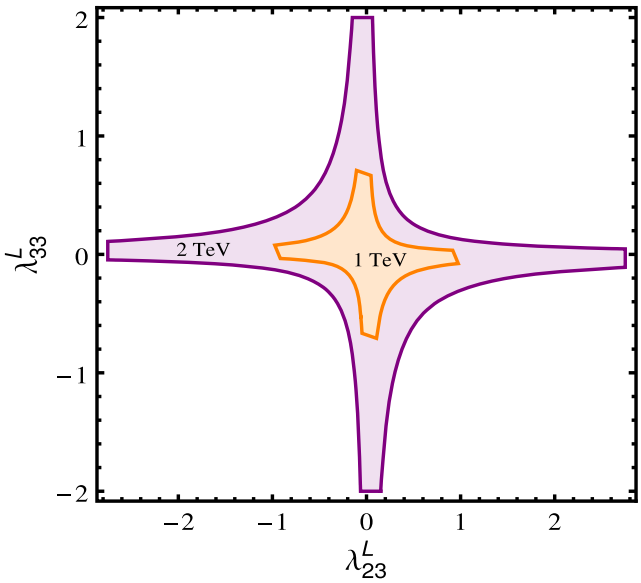

FIG. 5. The region where $R^{\nu\nu}_{K^*} < 2.7$ for $M_{S_1} = 1$ and 2 TeV.

D. Constraint from $Z \to \tau\tau$ decay

Another important constraint comes from the $Z\tau\tau$ coupling measurements. The $Z \to \tau\tau$ decay is affected by the S_1 loops as shown in Ref. [47]. The contribution of S_1 to the $Z\tau\tau$ coupling shift ($\Delta\kappa_{Z\tau\tau}$) comes from a loop with an up-type quark (q) and an S_1. The shift scales as the square of the $S_1 t\tau$ coupling ($\lambda^{L/R}_{q3}$) and m_q^2. Hence, the dominant contribution comes from when q is the top quark implying that the $Z\tau\tau$ coupling measurements can restrict only λ^L_{33} but not λ^L_{23} or λ^R_{23}. For instance, we see from Ref. [47] that $\lambda^L_{33} \gtrsim 1.4$ can be excluded for $M_{S_1} \sim 1$ TeV with 2σ confidence. We incorporate this bound into our parameter scan.

E. LHC phenomenology and constraints

We now make a quick survey of the relevant LHC phenomenology of a TeV-range S_1 that couples with τ, ν and s and c quarks. For this discussion we compute all the necessary cross sections using the universal FeynRules output [94] model files from Ref. [48] in MADGRAPH5 [95]. We use the NNPDF23LO [96] parton distribution functions. Wherever required, we include the next-to-leading-order QCD K-factor of ~1.3 for the pair production in our analysis [97].

1. Decay modes of S_1

For nonzero λ^L_{23}, λ^L_{33} and λ^R_{23}, S_1 can decay to $c\tau$, $s\nu$, $t\tau$ and $b\nu$ states. CKM mixing among quarks enables decays to $u\tau$ and $d\nu$ but we neglect them in our analysis as the off-diagonal CKM elements are small. The BRs of S_1 to various decay modes vary depending on the coupling strengths. If $\lambda^R_{23} \gg \lambda^L_{23}, \lambda^L_{33}$, the dominant decay mode is $S_1 \to c\tau$, whereas for $\lambda^L_{23} \gg \lambda^R_{23}, \lambda^L_{33}$, $\mathrm{BR}(S_1 \to c\tau) \approx \mathrm{BR}(S_1 \to s\nu) \approx 50\%$. On the other hand, when $\lambda^L_{33} \gg \lambda^L_{23}, \lambda^R_{23}$, the dominant decay modes are $S_1 \to t\tau$ and $S_1 \to b\nu$ with about a 50% BR in each mode. Since partial decay widths depend linearly on M_{S_1}, BRs are insensitive to the mass of S_1.

2. Production of S_1

At the LHC, S_1 can be produced resonantly in pairs or singly and nonresonantly through indirect production (t-channel S_1 exchange process).

Pair production: The pair production of S_1 is dominated by the strong coupling and, therefore, it is almost model independent. The mild model dependence enters in the pair production through the t-channel lepton or neutrino exchange processes. However, the amplitudes of those diagrams are proportional to λ^2 and generally suppressed for small λ values (for bigger M_{S_1} and large λ values, this part could be comparable to the model-independent part of the pair production). Pair production is heavily phase-space suppressed for large M_{S_1} and we find that its contribution is very small in our recast analysis. Pair production can be categorized into two types depending on the final states: symmetric, where both leptoquarks decay to the same modes, and asymmetric, where the two leptoquarks decay via two different modes. These two types give rise to various novel final states.

Symmetric modes:

$$S_1 S_1 \to \widehat{c\tau}\,\widehat{c\tau} \equiv \tau\tau + 2j, \qquad \widehat{t\tau}\,\widehat{t\tau} \equiv tt + \tau\tau, \qquad \widehat{s\nu}\,\widehat{s\nu} \equiv 2j + \not{E}_{\mathrm{T}}, \qquad \widehat{b\nu}\,\widehat{b\nu} \equiv 2b + \not{E}_{\mathrm{T}}.$$

Asymmetric modes:

$$S_1 S_1 \to \widehat{c\tau}\,\widehat{s\nu} \equiv \tau + 2j + \not{E}_{\mathrm{T}}, \qquad \widehat{c\tau}\,\widehat{b\nu} \equiv \tau + b + j + \not{E}_{\mathrm{T}}, \qquad \widehat{c\tau}\,\widehat{t\tau} \equiv \tau\tau + t + j,$$
$$S_1 S_1 \to \widehat{s\nu}\,\widehat{b\nu} \equiv b + j + \not{E}_{\mathrm{T}}, \qquad \widehat{s\nu}\,\widehat{t\tau} \equiv t + \tau + j + \not{E}_{\mathrm{T}}, \qquad \widehat{b\nu}\,\widehat{t\tau} \equiv t + \tau + b + \not{E}_{\mathrm{T}},$$

where the curved connection over a pair of particles indicates that the pair is coming from a decay of S_1. Searches for leptoquarks in some of the symmetric modes were already done at the LHC [87,88]. Leptoquark searches in some of the symmetric and most of the asymmetric modes are yet to be performed at the LHC.

Single production: The single productions of S_1, where S_1 is produced in association with a SM particle, are fully model dependent as they depend on the leptoquark-quark-lepton couplings. These are important production modes for large couplings and heavier masses (since single productions receive less phase-space suppression than the pair production). Depending on the final states, single productions can be categorized as follows.

Symmetric modes:

$$\mathcal{S}_1\tau X \to \overset{\frown}{\tau c}\tau + \overset{\frown}{\tau c}\tau j\,(+\overset{\frown}{\tau c}\tau jj + \cdots) \equiv \tau\tau + \text{jets},$$
$$\mathcal{S}_1\tau X \to \overset{\frown}{\tau t}\tau + \overset{\frown}{\tau t}\tau j\,(+\overset{\frown}{\tau t}\tau jj + \cdots) \equiv \tau\tau + t + \text{jets},$$
$$\mathcal{S}_1\nu X \to \overset{\frown}{\nu s}\nu + \overset{\frown}{\nu s}\nu j\,(+\overset{\frown}{\nu s}\nu jj + \cdots) \equiv \not{E}_{\mathrm{T}} + \text{jets},$$
$$\mathcal{S}_1\nu X \to \overset{\frown}{\nu b}\nu + \overset{\frown}{\nu b}\nu j\,(+\overset{\frown}{\nu b}\nu jj + \cdots) \equiv \not{E}_{\mathrm{T}} + b + \text{jets}.$$

Asymmetric modes:

$$S_1\tau X \to \overset{\frown}{\nu s}\tau + \overset{\frown}{\nu s}\tau j\,(+\overset{\frown}{\nu s}\tau jj + \cdots) \equiv \not{E}_{\mathrm{T}} + \tau + \text{jets},$$
$$S_1\nu X \to \overset{\frown}{\tau c}\nu + \overset{\frown}{\tau c}\nu j\,(+\overset{\frown}{\tau c}\nu jj + \cdots) \equiv \not{E}_{\mathrm{T}} + \tau + \text{jets},$$
$$S_1\tau X \to \overset{\frown}{\nu b}\tau + \overset{\frown}{\nu b}\tau j\,(+\overset{\frown}{\nu b}\tau jj + \cdots) \equiv \not{E}_{\mathrm{T}} + \tau + b + \text{jets},$$
$$S_1\nu X \to \overset{\frown}{\tau t}\nu + \overset{\frown}{\tau t}\nu j\,(+\overset{\frown}{\tau t}\nu jj + \cdots) \equiv \not{E}_{\mathrm{T}} + \tau + t + \text{jets}.$$

Here j stands for an untagged jet and "jets" means any number (≥ 1) of untagged jets. These extra jets can be either radiation or hard (genuine three-body single production processes can have sizeable cross sections; see Refs. [98–100] for how one can systematically compute them). As single production is model dependent, the relative strengths of these modes depend on the relative strengths of the coupling involved in the production as well as the BR of the decay mode involved.

Indirect production: Indirect production is the nonresonant process where a leptoquark is exchanged in the t channel. With leptoquark couplings to τ and ν, this basically gives rise to three possible final states: $\tau\tau(\tau\tau + \text{jets})$, $\tau\nu(\not{E}_{\mathrm{T}} + \tau + \text{jets})$ and $\nu\nu(\not{E}_{\mathrm{T}} + \text{jets})$. The amplitudes of these processes are proportional to λ^2. So the cross section grows as λ^4. Hence, for an order-one λ, indirect production has a larger cross section than other production processes for large M_{S_1} (see Fig. 2 of Ref. [48]). However, the indirect production substantially interferes with the SM background process $pp \to V^{(*)} \to \ell\ell$ ($\ell = \tau/\nu$). Though the interference is $\mathcal{O}(\lambda^2)$, its contribution can be significant for a TeV-scale S_1 because of the large SM contribution (larger than both the direct production modes and the λ^4 indirect contribution, assuming $\lambda \gtrsim 1$). In general, the interference could be either constructive or destructive depending on the nature of the leptoquark species and its mass [101]. For S_1, we find that the interference is destructive in nature [48]. Hence, for a TeV-scale S_1 if λ is large, this destructive interference becomes its dominant signature in the leptonic final states.

3. Constraints from the LHC

The mass exclusion limits from the pair-production searches for S_1 at the LHC are as follows. Assuming a 100% BR in the $S \to t\tau$ mode, a recent search at the CMS detector has excluded masses below 900 GeV [87]. Similarly, for a leptoquark that decays exclusively to $b\nu$ or $s\nu(\equiv j\nu)$ final states, the exclusion limits are at 1100 and 980 GeV [88], respectively. However, going beyond simple mass exclusions, we make use of the analysis done in Ref. [48] for the LHC constraints. It contains the independent LHC limits on the three couplings shown in Eq. (17) as functions of M_{S_1} as well as a summery of the direct-detection exclusion limits.

Apart from the processes with $\not{E}_{\mathrm{T}} + \text{jets}$ final states, all other production processes can have either $\tau\tau + \text{jets}$ final states or $\not{E}_{\mathrm{T}} + \tau + \text{jets}$ final states. Hence, the latest $pp \to Z' \to \tau\tau$ and $pp \to W' \to \tau\nu$ searches at the ATLAS detector [102,103] were used to derive the constraints in Ref. [48]. There we notice that the limits on λ^L_{23} from the $\tau\nu$ data are weaker that the ones obtained from the $\tau\tau$ data. The $\tau\tau$ data also constrain λ^R_{23}. From the earlier discussion, it is clear that the interference contribution plays the dominant role in determining these limits. However, its destructive nature means that in the signal region one would expect less events than in the SM-only predictions. Hence, the limits

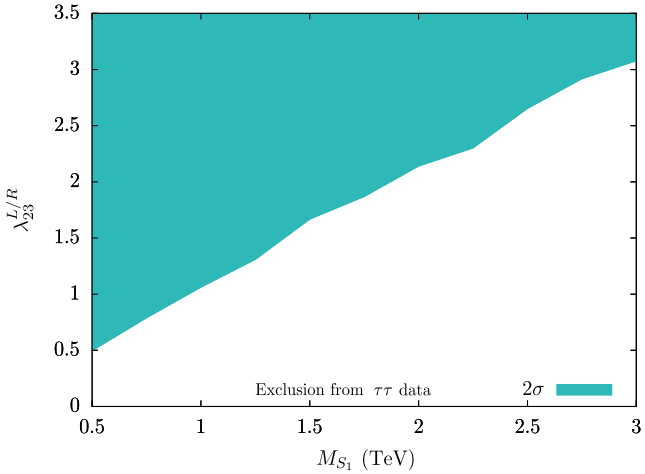

FIG. 6. Two-sigma exclusion limits on $\lambda_{23}^{L/R} = \sqrt{(\lambda_{23}^L)^2 + (\lambda_{23}^R)^2}$ as a function of M_{S_1} as obtained in Ref. [48] from the ATLAS $pp \to \tau\tau$ data [102]. The colored region is excluded.

were obtained assuming that either λ_{23}^L or λ_{23}^R is nonzero at a time or by performing a χ^2 test of the transverse mass ($m_{\rm T}$) distributions of the data. As, for heavy S_1, the limits on λ_{23}^L and λ_{23}^R are dominantly determined by the interference of the indirect production, they are very similar. We can translate these limits from the $\tau\tau$ data on any combination of λ_{23}^L and λ_{23}^R in a simple manner assuming $\lambda_{23}^{L/R} = \sqrt{(\lambda_{23}^L)^2 + (\lambda_{23}^R)^2}$. In Fig. 6 we display the limits on $\lambda_{23}^{L/R}$ as a function of M_{S_1}.[4]

The LHC data is insensitive to λ_{33}^L as it was shown in Ref. [48]. This can be understood from the following argument. First, the pair production is insensitive to this coupling as we have already mentioned. Second, the single-production process $pp \to t\tau\nu$ via an S_1 has too small a cross section ($\sim$2 fb for $\lambda_{33}^L \sim 1$ and $M_{S_1} = 1$ TeV) to make any difference at the present luminosity. Finally, there is no interference contribution in the $\tau\tau$ and $\tau + \not{E}_{\rm T}$ channels as there is no t quark in the initial state. Hence, λ_{33}^L remains unbounded from these searches.

F. Parameter scan

To find the $R_{D^{(*)}}$-favored regions in the S_1 parameter space that are not in conflict with the limits on $F_L(D^*)$, $P_\tau(D^*)$, $R_{K^{(*)}}^{\nu\nu}$, $Z \to \tau\tau$ decay and the bounds from the LHC, we consider two benchmark leptoquark masses: $M_{S_1} = 1$ and 2 TeV. We allow all three free couplings, λ_{23}^L, λ_{23}^R and λ_{33}^L to vary. For every benchmark mass, we perform a random scan over the three couplings in the perturbative range $-\sqrt{4\pi}$ to $\sqrt{4\pi}$ (i.e., $|\lambda|^2/4\pi \leq 1$). We do not consider complex values for the couplings. In Fig. 7, we show the outcome of our scan with different two-dimensional projections. In every plot we show two couplings and allow the third coupling to vary. In each of these plots we show the following.

(1) *The flavor ∪ EW (FEW) regions:* The orange dots mark the regions favored by the $R_{D^{(*)}}$ observables within 95% C.L. while satisfying the available bounds on the $F_L(D^*)$, $P_\tau(D^*)$ and $R_{K^{(*)}}^{\nu\nu}$ observables (flavor bounds). In addition, these points also satisfy the bound on λ_{33}^L coming from the $Z \to \tau\tau$ decay within 95% C.L. [47] (electroweak bound).

(2) *The flavor ∪ EW ∪ LHC (FEWL) regions:* As we take into account the limits on $\lambda_{23}^{L/R}$ from the ATLAS $pp \to \tau\tau$ data from the 13 TeV LHC [48] along with the previous constraints we obtain the regions marked by the green points. These are the points that survive all the limits considered in this paper.

From the plots we see that substantial portions of parameter regions survive after all the constraints. This implies that the S_1 model can successfully explain the $R_{D^{(*)}}$ anomalies. If one looks only at the $R_{D^{(*)}}$ anomalies, in principle, one can just set λ_{23}^L and/or λ_{33}^L to be large. But coupling values that make C_{V_L} [see Eq. (23)] big come into conflict with the $R_{K^{(*)}}^{\nu\nu}$ bound [see Eq. (34)]. This is why we do not see any point where both λ_{23}^L and λ_{33}^L are large in the first column of Fig. 7. In addition, the LHC puts bounds on $\lambda_{23}^{L/R}$ [48] whereas the $Z \to \tau\tau$ data puts a complimentary bound on λ_{33}^L [47]. The restriction on λ_{33}^L from the $Z \to \tau\tau$ data can be seen in Figs. 7(a) and 7(c) for $M_{S_1} = 1$ TeV and Figs. 7(d) and 7(f) for $M_{S_1} = 2$ TeV, whereas from the middle column [i.e., Figs. 7(b) and 7(e)] it is clear that the LHC prevents both λ_{23}^L and λ_{23}^R from taking large values simultaneously. From the λ_{23}^R vs λ_{33}^L plots [Figs. 7(c) and 7(f)] we see that these two couplings take opposite signs mainly because both R_{D^*} and $F_L(D^*)$ prefer a positive C_{S_L} [see Eqs. (28) and (31)].

G. RG running of the Yukawa couplings and perturbativity

One of the questions raised by the introduction of new Yukawa couplings is whether the new model remains perturbative up to high-enough energies. This is particularly important in the GUT framework since the RG running of the gauge couplings is performed under the assumption of perturbativity. Fortunately, with the latest LHC data, we have quite a large available parameter space in the deep perturbative region, as can be seen in Fig. 7. While this suggests that the model is safe in terms of perturbativity as long as the new Yukawa couplings are small enough at the electroweak scale, it is still informative to investigate the RG running in detail, especially the case

[4]Actually, for M_{S_1} between 1 and 2 TeV, the limits on λ_{23}^L are slightly stronger than those on λ_{23}^R because in the SM the Z boson couples differently to left- and right-handed τ's. However, we ignore this minor difference and take the stronger limits on λ_{23}^L as the limits on $\lambda_{23}^{L/R}$ to remain conservative.

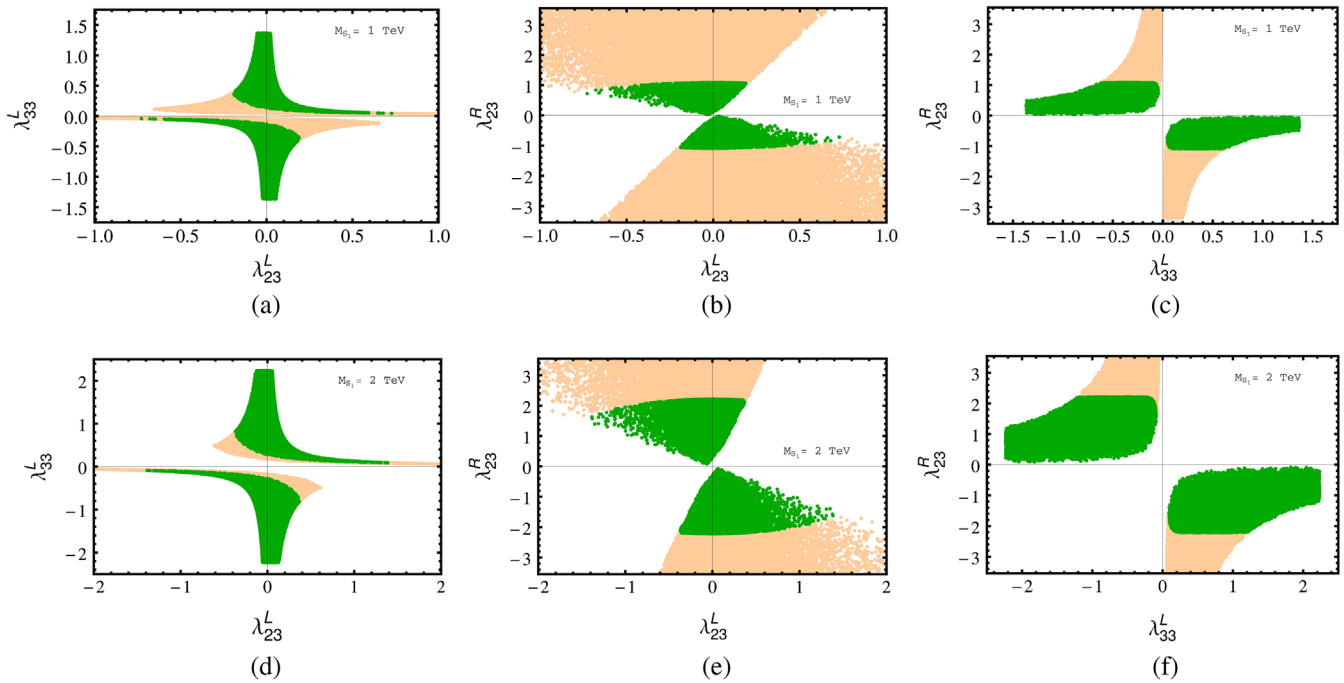

FIG. 7. Two-dimensional projections of the regions in the S_1 parameter space allowed by the bounds on the $R_{D^{(*)}}$, $F_L(D^*)$, $P_\tau(D^*)$ and $R^{\nu\nu}_{K^{(*)}}$ observables and the $Z \to \tau\tau$ decay, i.e., the FEW regions (orange) (see Sec. IV F), and the LHC constraints in addition to all these constraints, i.e., the FEWL regions (green) for $M_{S_1} = 1$ TeV (upper panel) and $M_{S_1} = 2$ TeV (lower panel). We assume all the couplings are real.

in which the Yukawa couplings take larger initial values. We address this issue in this part of the paper.[5]

The equations for the RG running of the Yukawa couplings are given in the Appendix. Results for various benchmark cases are displayed in Fig. 8. Among the S_1 mass values we have considered in this paper, the most constrained parameter space is that of $M_{S_1} = 2$ TeV. Therefore, we choose our benchmark values from the parameter space for this mass value, displayed in Fig. 7. Note that $\lambda^L_{33}(M_Z)$ and $\lambda^L_{23}(M_Z)$ cannot both be large and that $\lambda^L_{33}(M_Z)$ and $\lambda^R_{23}(M_Z)$ must have opposite signs, as can be seen in Fig. 7. When $\lambda^L_{23}(M_Z)$ is taken in the interval $[-0.2, 0.1]$, the system remains perturbative up to the grand unification scale, $\sim 10^{15}$–10^{17} GeV, even when $|\lambda^L_{33}(M_Z)|$, $|\lambda^R_{23}(M_Z)| \approx 1$, as displayed in the first six plots in Fig. 8. However, it deteriorates quickly for larger values of $|\lambda^L_{33}(M_Z)|$ and $|\lambda^R_{23}(M_Z)|$ [Fig. 8(g)]. When $|\lambda^L_{23}(M_Z)|$ is large, the parameter space is quite limited for $|\lambda^L_{33}(M_Z)|$, which is in the [0.10, 0.15] band (Fig. 7). In this case as well, the system is well behaved up to $|\lambda^L_{23}(M_Z)|$, $|\lambda^R_{23}(M_Z)| \approx 1$ [e.g., Fig. 8(h)], and the situation declines for the values above in that the perturbativity bound is reached below the unification scale [e.g., Fig. 8(i)].

[5]A perturbativity analysis for the case of the Standard Model augmented by a leptoquark S_1 was done in Ref. [80], as well. Note that their Yukawa matrix is flavor diagonal, and hence different from the one in this paper.

Note that although we perform the Yukawa RG running based on the SM augmented with a TeV-scale leptoquark S_1 all the way up to the UV, these equations are prone to changes above the intermediate symmetry-breaking scale provided that there is one (as in the examples studied in Sec. III), mainly due to contributions from the running of the scalars whose masses are around the intermediate scale. However, these effects are expected to be minor due to the corresponding beta-function coefficients not being large enough to significantly change the logarithmic RG running [71]. This is even more likely to be the case especially if this symmetry-breaking scale, for instance the scale in our scenario where the Pati-Salam symmetry is spontaneously broken to the symmetry of the SM, is considerably close to the scale of the SO(10) symmetry-breaking scale (as in the second case in Sec. III, namely model A_2), suggesting that the supposed modification in the Yukawa running is indeed not an issue of concern since the slow logarithmic running would most likely not significantly alter the outcome in this small interval. Threshold corrections due to the intermediate scale are also known to be subleading to the one-loop running [75].

Furthermore, although we have studied some specific examples for gauge coupling unification, there are no restrictions on the choice of the mass values of the high-energy field content regarding which fields remain heavy at the unification scale and which ones slide through the intermediate scale, as long as the gauge coupling

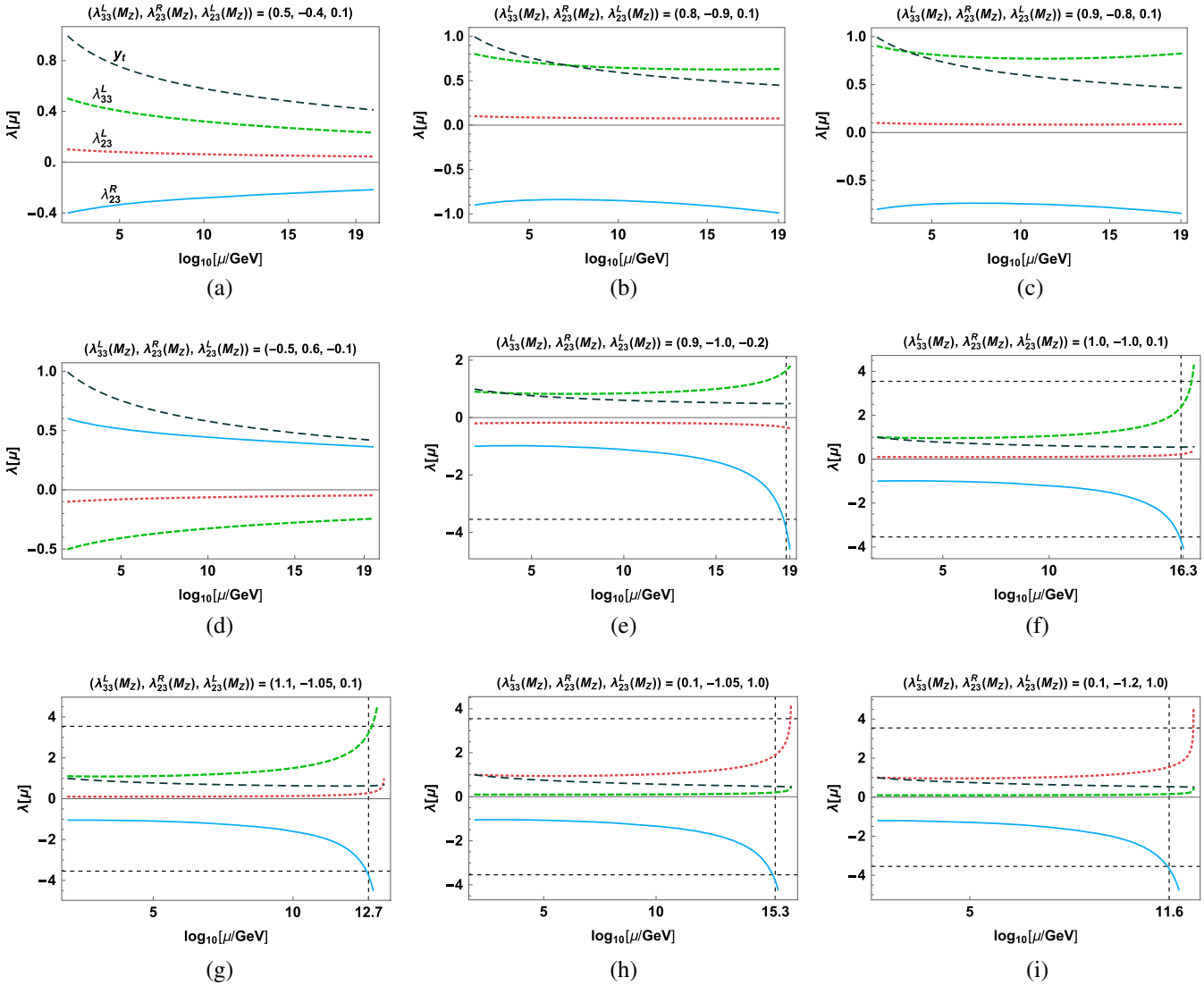

FIG. 8. Behavior of Yukawa couplings with various benchmark values at the EW scale. The labels of the couplings are given in the first plot. The dashed horizontal lines denote the values of the assumed perturbativity bound, $\pm\sqrt{4\pi}$. The dashed vertical line denotes the energy scale at which this bound is first reached.

unification is realized (and as long as the intermediate scale is high enough to evade the proton-decay constraints for the terms not forbidden by any symmetry in the Lagrangian). The main point of our case that we emphasize is that if a SO(10) theory is indeed the UV completion of the SM, then one may naturally anticipate a TeV-scale leptoquark accompanying the SM Higgs field, and this could define the field content up to very high energies. Beyond that, one has the freedom to choose the high-energy particle content and the corresponding potential terms in the Lagrangian that lead to an appropriate symmetry-breaking sequence in which the Yukawa couplings remain in the perturbative realm above the intermediate symmetry-breaking scale. With this in mind, even the other cases, displayed in Figs. 8(g) and 8(i), that suffer from the perturbativity problem at relatively low energies could arguably get a pass, as long as the high-energy content of the theory is chosen such that the intermediate symmetry breaking occurs before the perturbativity bound is reached and such that the couplings remain in the perturbative realm up to the unification scale.

We comment in passing on the unification-scale implications of our model regarding the fermion mass spectrum. It has been known in the literature that obtaining a realistic Yukawa sector in the SO(10) framework is not trivial. None of the single- and dual-field combinations of the scalar fields $\mathbf{10}_H$, $\mathbf{120}_H$, and $\mathbf{126}_H$ yields GUT-scale relations between fermion masses consistent with the SM values [68,75]. On the other hand, it was concluded in Ref. [75] that a Higgs sector consisting of a real $\mathbf{10}_H$, a real $\mathbf{120}_H$, and a complex $\mathbf{126}_H$ can provide a fermion mass spectrum at the unification scale that matches the expected values

TABLE V. Fermion masses at the unification scale $M_U = 2 \times 10^{16}$ GeV that are selected for the sake of argument as the exponential midpoint of the unification scales of the high-energy scenarios discussed in Sec. III. Clearly, inclusion of S_1 in the low-energy particle spectrum does not lead to significant changes in the fermion mass values at the unification scale compared to the SM predictions, especially in the deep perturbative region in the $(\lambda_{33}^L, \lambda_{23}^R, \lambda_{23}^L)$ parameter space.

$(\lambda_{33}^L, \lambda_{23}^R, \lambda_{23}^L)$ Fermion masses/ratios	(0,0,0); SM	$(0.5, -0.4, 0.1)$	$(0.8, -0.9, 0.1)$	$(0.1, -1.0, 1.0)$
m_t/m_b	75.57	75.66	76.37	75.36
m_τ/m_b	1.63	1.74	2.31	4.28
m_μ/m_s	4.41	4.46	4.46	3.94
m_e/m_d	0.400	0.401	0.401	0.401
m_t/GeV	79.32	79.52	83.46	78.14
m_c/GeV	0.254	0.254	0.275	0.344
$m_\mu/(10^{-3}$ GeV)	100.505	100.576	101.518	100.175
$m_e/(10^{-3}$ GeV)	0.476	0.476	0.481	0.475
$m_u/(10^{-3}$ GeV)	0.469	0.464	0.469	0.462

obtained by the RG running of the SM with small threshold corrections at the intermediate scale. Since this is the scalar sector we adopt in this paper, it is informative to inspect whether the light leptoquark S_1 can register significant changes to the expected fermion mass values at the unification scale obtained via the SM RG running.

The results, obtained by using the equations given in the Appendix and the same values for the input parameters at M_Z as in Ref. [75], are given in Table V, some of which are displayed in terms of mass ratios relevant in the SO(10) framework. The unification scale is selected as $M_U = 2 \times 10^{16}$ GeV, which is around the exponential midpoint of the unification scales of our models A_1 and A_2 discussed in Sec. III; small numerical differences depending on the M_U value in that range are not relevant to our discussion here. Our values for the fermion masses at M_U in the SM case differ from the ones in Ref. [75] by 1–5%, which might be due to a combination of effects coming from the running of the right-handed neutrinos above the intermediate scale and the threshold corrections, both of which are ignored in our estimation.[6] The results for the leptoquark case are given for three benchmark points in the $(\lambda_{33}^L, \lambda_{23}^R, \lambda_{23}^L)$ parameter space that are consistent with the perturbativity analysis above. As expected, when all three of the new Yukawa couplings are in the deep perturbative region, the differences from the SM values remain insignificant. When the couplings get larger close to unity, some deviations are observed yet they do not become substantial. Therefore, we conclude that the addition of S_1 to the particle content up to the TeV scale does not lead to significant changes regarding the expected fermion masses at the unification scale and therefore the analysis of Ref. [75], based on using the extrapolated SM values at the unification scale as input data in order to numerically fit them to the parameters of the Yukawa sector of their SO(10) model, can be applied in our case as well.

[6]We do not discuss neutrino masses in this paper but have no reason to suspect that the outcome would be different than that in Ref. [75] particularly because their intermediate symmetry-breaking scales at which the generation of neutrino masses through the seesaw mechanism occurs are quite close to the ones in our models A_1 and A_2.

V. SUMMARY AND DISCUSSIONS

In this paper, we considered the scenario that there is a single scalar leptoquark, S_1, at the TeV scale, and it is the color-triplet component of a real **10** of SO(10), which also contains a SU(2) doublet which is identified as the SM Higgs. In this scenario, the leptoquark being the only scalar entity other than the SM Higgs is natural; a peculiar mass splitting between the components of **10** does not occur and the leptoquark picks up an electroweak-scale mass together with the SM Higgs, as expected. This is appealing because this leptoquark by itself can potentially explain the B-decay anomalies at the LHC [21,22,25,32].

The SO(10) grand unification framework is an appealing scenario, which has been heavily studied in the literature [62,64–75]. It unifies the three forces in the SM, explains the quantization of electric charge, provides numerous dark matter candidates, accommodates a seesaw mechanism for small neutrino masses, and justifies the remarkable cancellation of anomalies through the anomaly-free nature of the SO(10) gauge group. Moreover, the fermionic content of the SM fits elegantly in $\mathbf{16}_F$, including a right-handed neutrino for each family. The particles in the SM (except probably the neutrinos) acquire masses up to the electroweak scale through interacting with the electroweak-scale Higgs field, which is generally assigned to a real $\mathbf{10}_H$. Considering that the leptoquark S_1 is the only other component in $\mathbf{10}_H$, a TeV-scale S_1, from this perspective, is consistent with the idea that it is the last piece of the

puzzle regarding the particle content up to the electroweak scale (modulo the right-handed neutrinos). Therefore, the possible detection of S_1, in the absence of any other new particles, at the TeV scale could be interpreted as evidence in favor of SO(10) grand unification.

One obvious issue of concern is proton decay since the leptoquark S_1 possesses the right quantum numbers for it to couple to potentially dangerous diquark operators. On the other hand, the proton stability could possibly be ensured through various mechanisms [22,38,68,76–78]. In this paper, we ensured the proton stability by assuming a discrete symmetry that is imposed in an *ad hoc* manner below the Pati-Salam breaking scale. It would certainly be more compelling to realize a similar mechanism at the fundamental level although it seems unlikely that it would interfere with the bottom line of this work.

Having a single S_1 leptoquark at the TeV scale as the only new physics remnant from our SO(10) GUT model, we investigated how competent this S_1 is at addressing the $R_{D^{(*)}}$ anomalies while simultaneously satisfying other relevant constraints from flavor, electroweak and direct LHC searches. We adopted a specific Yukawa coupling texture with only three free (real) nonzero couplings viz. λ^L_{23}, λ^L_{33} and λ^R_{23}. We have found that this minimal consideration can alleviate the potential tension between the $R_{D^{(*)}}$-favored region and the $R^{\nu\nu}_{K^{(*)}}$ measurements. The $Z \to \tau\tau$ decay constrains λ^L_{33} whereas the $\tau\tau$ resonance search at the LHC puts complimentary bounds on λ^L_{23} and λ^R_{23}. By combining these constraints with all the relevant flavor constraints coming from the latest data on $R_{D^{(*)}}$, $F_L(D^*)$, $P_\tau(D^*)$, $R^{\nu\nu}_{K^{(*)}}$ we have found that a substantial region of the $R_{D^{(*)}}$-favored parameter space is allowed. Our multiparameter analysis clearly shows that contrary to the common perception, a single leptoquark solution to the observed $R_{D^{(*)}}$ anomalies with S_1 is still a viable solution.

Evidently, by introducing new d.o.f. into our framework, one can, *a priori*, enlarge the allowed parameter region. For example, by considering some of the couplings as complex or by choosing a complex (instead of a real) **10** representation of SO(10), which will introduce an additional S_1 and another complex scalar doublet at the TeV scale, one can relax our obtained bounds. We also pointed out search strategies for S_1 at the LHC using symmetric and asymmetric pair- and single-production channels. Systematic studies of these channels are discussed elsewhere [104].

ACKNOWLEDGMENTS

We thank Diganta Das for valuable discussions and collaboration in the early stages of the project. Work of U. A. is supported in part by the Chinese Academy of Sciences President's International Fellowship Initiative (PIFI) under Grant No. 2020PM0019; the Institute of High Energy Physics, Chinese Academy of Sciences, under Contract No. Y9291120K2; and the National Natural Science Foundation of China (NSFC) under Grant No. 11505067. T. M. is financially supported by the Royal Society of Arts and Sciences of Uppsala as a researcher at Uppsala University and by the INSPIRE Faculty Fellowship of the Department of Science and Technology (DST) under Grant No. IFA16-PH182 at the University of Delhi. S. M. acknowledges support from the Science and Engineering Research Board (SERB), DST, India under Grant No. ECR/2017/000517.

APPENDIX: RENORMALIZATION GROUP RUNNING OF THE YUKAWA COUPLINGS

The new Yukawa matrices in the Lagrangian given in Eq. (9) are taken in our setup as

$$\Lambda^L \to \begin{pmatrix} 0 & 0 & 0 \\ 0 & 0 & \lambda^L_{23} \\ 0 & 0 & \lambda^L_{33} \end{pmatrix} \quad \text{and} \quad \Lambda^R \to \begin{pmatrix} 0 & 0 & 0 \\ 0 & 0 & \lambda^R_{23} \\ 0 & 0 & 0 \end{pmatrix}. \tag{A1}$$

Following Ref. [105] (or implementing the model in SARAH [106]), the corresponding one-loop RG equations can be found as

$$16\pi^2\beta_{\lambda^R_{23}} = 3(\lambda^R_{23})^3 - \lambda^R_{23}\left(\frac{13}{3}g_1^2 + 4g_3^2\right) + 2\lambda^R_{23}((\lambda^L_{23})^2 + (\lambda^L_{33})^2), \tag{A2}$$

$$16\pi^2\beta_{\lambda^L_{33}} = 4(\lambda^L_{33})^3 - \lambda^L_{33}\left(-\frac{y_t^2}{2} + \frac{5}{6}g_1^2 + \frac{9}{2}g_2^2 + 4g_3^2\right) + \lambda^L_{33}((\lambda^R_{23})^2 + 4(\lambda^L_{23})^2), \tag{A3}$$

$$16\pi^2\beta_{\lambda^L_{23}} = 4(\lambda^L_{23})^3 - \lambda^L_{23}\left(\frac{5}{6}g_1^2 + \frac{9}{2}g_2^2 + 4g_3^2\right) + \lambda^L_{23}((\lambda^R_{23})^2 + 4(\lambda^L_{33})^2), \tag{A4}$$

$$16\pi^2\beta_{y_t} = 3y_t^3 + y_t\left(\frac{3}{2}y_t^3 - \frac{17}{12}g_1^2 - \frac{9}{4}g_2^2 - 8g_3^2\right) + \frac{1}{2}y_t(\lambda^L_{33})^2, \tag{A5}$$

$$16\pi^2\beta_{y_c} = y_c\left(3y_t^2 - \frac{17}{12}g_1^2 - \frac{9}{4}g_2^2 - 8g_3^2\right) + \frac{1}{2}y_c((\lambda^R_{23})^2 + (\lambda^L_{23})^2), \tag{A6}$$

$$16\pi^2\beta_{y_u} = y_u\left(3y_t^2 - \frac{17}{12}g_1^2 - \frac{9}{4}g_2^2 - 8g_3^2\right), \tag{A7}$$

$$16\pi^2\beta_{y_b} = y_b\left(\frac{3}{2}y_t^2 - \frac{5}{12}g_1^2 - \frac{9}{4}g_2^2 - 8g_3^2\right) + \frac{1}{2}y_b(\lambda_{33}^L)^2, \tag{A8}$$

$$16\pi^2\beta_{y_s} = y_s\left(3y_t^2 - \frac{5}{12}g_1^2 - \frac{9}{4}g_2^2 - 8g_3^2\right) + \frac{1}{2}y_s(\lambda_{23}^L)^2, \tag{A9}$$

$$16\pi^2\beta_{y_d} = y_d\left(3y_t^2 - \frac{5}{12}g_1^2 - \frac{9}{4}g_2^2 - 8g_3^2\right), \tag{A10}$$

$$16\pi^2\beta_{y_e} = y_e\left(3y_t^2 - \frac{15}{4}g_1^2 - \frac{9}{4}g_2^2\right), \tag{A11}$$

$$16\pi^2\beta_{y_\mu} = y_\mu\left(3y_t^2 - \frac{15}{4}g_1^2 - \frac{9}{4}g_2^2\right), \tag{A12}$$

$$16\pi^2\beta_{y_\tau} = y_\tau\left(3y_t^2 - \frac{15}{4}g_1^2 - \frac{9}{4}g_2^2\right) + \frac{3}{2}y_\tau((\lambda_{23}^R)^2 + (\lambda_{23}^L)^2 + (\lambda_{33}^L)^2), \tag{A13}$$

where $\beta_y \equiv \mu\frac{dy}{d\mu}$ and the RG running of the gauge couplings are performed in the usual way according to Eq. (10). In the Yukawa running above, only the dominant terms are taken into account since the subleading ones are significantly suppressed and have no noticeable effects on our analysis.

[1] J. P. Lees *et al.* (*BABAR* Collaboration), Evidence for an Excess of $\bar{B} \to D^{(*)}\tau^-\bar{\nu}_\tau$ Decays, Phys. Rev. Lett. **109**, 101802 (2012).

[2] J. P. Lees *et al.* (*BABAR* Collaboration), Measurement of an excess of $\bar{B} \to D^{(*)}\tau^-\bar{\nu}_\tau$ decays and implications for charged Higgs bosons, Phys. Rev. D **88**, 072012 (2013).

[3] R. Aaij *et al.* (LHCb Collaboration), Test of Lepton Universality Using $B^+ \to K^+\ell^+\ell^-$ Decays, Phys. Rev. Lett. **113**, 151601 (2014).

[4] R. Aaij *et al.* (LHCb Collaboration), Test of lepton universality with $B^0 \to K^{*0}\ell^+\ell^-$ decays, J. High Energy Phys. 08 (2017) 055.

[5] R. Aaij *et al.* (LHCb Collaboration), Measurement of the Ratio of Branching Fractions $\mathcal{B}(\bar{B}^0 \to D^{*+}\tau^-\bar{\nu}_\tau)/\mathcal{B}(\bar{B}^0 \to D^{*+}\mu^-\bar{\nu}_\mu)$, Phys. Rev. Lett. **115**, 111803 (2015); Erratum, Phys. Rev. Lett. **115**, 159901(E) (2015).

[6] R. Aaij *et al.* (LHCb Collaboration), Measurement of the Ratio of the $B^0 \to D^{*-}\tau^+\nu_\tau$ and $B^0 \to D^{*-}\mu^+\nu_\mu$ Branching Fractions Using Three-Prong τ-Lepton Decays, Phys. Rev. Lett. **120**, 171802 (2018).

[7] R. Aaij *et al.* (LHCb Collaboration), Test of Lepton flavor universality by the measurement of the $B^0 \to D^{*-}\tau^+\nu_\tau$ branching fraction using three-prong τ decays, Phys. Rev. D **97**, 072013 (2018).

[8] M. Huschle *et al.* (Belle Collaboration), Measurement of the branching ratio of $\bar{B} \to D^{(*)}\tau^-\bar{\nu}_\tau$ relative to $\bar{B} \to D^{(*)}\ell^-\bar{\nu}_\ell$ decays with hadronic tagging at Belle, Phys. Rev. D **92**, 072014 (2015).

[9] Y. Sato *et al.* (Belle Collaboration), Measurement of the branching ratio of $\bar{B}^0 \to D^{*+}\tau^-\bar{\nu}_\tau$ relative to $\bar{B}^0 \to D^{*+}\ell^-\bar{\nu}_\ell$ decays with a semileptonic tagging method, Phys. Rev. D **94**, 072007 (2016).

[10] S. Hirose *et al.* (Belle Collaboration), Measurement of the τ Lepton Polarization and $R(D^*)$ in the Decay $\bar{B} \to D^*\tau^-\bar{\nu}_\tau$, Phys. Rev. Lett. **118**, 211801 (2017).

[11] S. Hirose *et al.* (Belle Collaboration), Measurement of the τ lepton polarization and $R(D^*)$ in the decay $\bar{B} \to D^*\tau^-\bar{\nu}_\tau$ with one-prong hadronic τ decays at Belle, Phys. Rev. D **97**, 012004 (2018).

[12] D. Bigi and P. Gambino, Revisiting $B \to D\ell\nu$, Phys. Rev. D **94**, 094008 (2016).

[13] F. U. Bernlochner, Z. Ligeti, M. Papucci, and D. J. Robinson, Combined analysis of semileptonic B decays to D and D^*: $R(D^{(*)})$, $|V_{cb}|$, and new physics, Phys. Rev. D **95**, 115008 (2017); Erratum, Phys. Rev. D **97**, 059902 (E) (2018).

[14] D. Bigi, P. Gambino, and S. Schacht, $R(D^*)$, $|V_{cb}|$, and the heavy quark symmetry relations between form factors, J. High Energy Phys. 11 (2017) 061.

[15] S. Jaiswal, S. Nandi, and S. K. Patra, Extraction of $|V_{cb}|$ from $B \to D^{(*)}\ell\nu_\ell$ and the standard model predictions of $R(D^{(*)})$, J. High Energy Phys. 12 (2017) 060.

[16] Y. Amhis *et al.* (HFLAV Collaboration), Averages of b-hadron, c-hadron, and τ-lepton properties as of summer 2016, Eur. Phys. J. C **77**, 895 (2017); We have used the spring 2019 averages from https://hflav-eos.web.cern.ch/hflav-eos/semi/spring19/html/RDsDsstar/RDRDs.html.

[17] G. Hiller and F. Kruger, More model-independent analysis of $b \to s$ processes, Phys. Rev. D **69**, 074020 (2004).

[18] M. Bordone, G. Isidori, and A. Pattori, On the standard model predictions for R_K and R_{K^*}, Eur. Phys. J. C **76**, 440 (2016).

[19] I. Doršner, S. Fajfer, N. Košnik, and I. Nišandžić, Minimally flavored colored scalar in $\bar{B} \to D^{(*)}\tau\bar{\nu}$ and the mass matrices constraints, J. High Energy Phys. 11 (2013) 084.

[20] Y. Sakaki, M. Tanaka, A. Tayduganov, and R. Watanabe, Testing leptoquark models in $\bar{B} \to D^{(*)}\tau\bar{\nu}$, Phys. Rev. D **88**, 094012 (2013).

[21] M. Freytsis, Z. Ligeti, and J. T. Ruderman, Flavor models for $\bar{B} \to D^{(*)}\tau\bar{\nu}$, Phys. Rev. D **92**, 054018 (2015).

[22] M. Bauer and M. Neubert, Minimal Leptoquark Explanation for the $R_{D^{(*)}}$, R_K, and $(g-2)_\mu$ Anomalies, Phys. Rev. Lett. **116**, 141802 (2016).

[23] B. Dumont, K. Nishiwaki, and R. Watanabe, LHC constraints and prospects for S_1 scalar leptoquark explaining the $\bar{B} \to D^{(*)}\tau\bar{\nu}$ anomaly, Phys. Rev. D **94**, 034001 (2016).

[24] D. Das, C. Hati, G. Kumar, and N. Mahajan, Towards a unified explanation of $R_{D^{(*)}}$, R_K and $(g-2)_\mu$ anomalies in a left-right model with leptoquarks, Phys. Rev. D **94**, 055034 (2016).

[25] D. Bečirević, N. Košnik, O. Sumensari, and R. Zukanovich Funchal, Palatable leptoquark scenarios for lepton flavor violation in exclusive $b \to s\ell_1\ell_2$ modes, J. High Energy Phys. 11 (2016) 035.

[26] D. Bečirević, S. Fajfer, N. Košnik, and O. Sumensari, Leptoquark model to explain the B-physics anomalies, R_K and R_D, Phys. Rev. D **94**, 115021 (2016).

[27] D. A. Faroughy, A. Greljo, and J. F. Kamenik, Confronting lepton flavor universality violation in B decays with high-p_T tau lepton searches at LHC, Phys. Lett. B **764**, 126 (2017).

[28] G. Hiller, D. Loose, and K. Schönwald, Leptoquark flavor patterns & B decay anomalies, J. High Energy Phys. 12 (2016) 027.

[29] C.-H. Chen, T. Nomura, and H. Okada, Excesses of muon $g-2$, $R_{D^{(*)}}$, and R_K in a leptoquark model, Phys. Lett. B **774**, 456 (2017).

[30] A. Crivellin, D. Müller, and T. Ota, Simultaneous explanation of $\mathrm{R}(\mathrm{D}^{(*)})$ and $b \to s\mu^+\mu^-$: The last scalar leptoquarks standing, J. High Energy Phys. 09 (2017) 040.

[31] D. Bečirević and O. Sumensari, A leptoquark model to accommodate $R_K^{\mathrm{exp}} < R_K^{\mathrm{SM}}$ and $R_{K^*}^{\mathrm{exp}} < R_{K^*}^{\mathrm{SM}}$, J. High Energy Phys. 08 (2017) 104.

[32] Y. Cai, J. Gargalionis, M. A. Schmidt, and R. R. Volkas, Reconsidering the One Leptoquark solution: flavor anomalies and neutrino mass, J. High Energy Phys. 10 (2017) 047.

[33] W. Altmannshofer, P. Bhupal Dev, and A. Soni, $R_{D^{(*)}}$ anomaly: A possible hint for natural supersymmetry with R-parity violation, Phys. Rev. D **96**, 095010 (2017).

[34] N. Assad, B. Fornal, and B. Grinstein, Baryon number and lepton universality violation in leptoquark and diquark models, Phys. Lett. B **777**, 324 (2018).

[35] M. Jung and D. M. Straub, Constraining new physics in $b \to c\ell\nu$ transitions, J. High Energy Phys. 01 (2019) 009.

[36] A. Biswas, D. K. Ghosh, S. K. Patra, and A. Shaw, $b \to c\ell\nu$ anomalies in light of extended scalar sectors, Int. J. Mod. Phys. A **34**, 1950112 (2019).

[37] P. Bandyopadhyay and R. Mandal, Revisiting scalar leptoquark at the LHC, Eur. Phys. J. C **78**, 491 (2018).

[38] U. Aydemir, D. Minic, C. Sun, and T. Takeuchi, B-decay anomalies and scalar leptoquarks in unified Pati-Salam models from noncommutative geometry, J. High Energy Phys. 09 (2018) 117.

[39] D. Marzocca, Addressing the B-physics anomalies in a fundamental composite Higgs model, J. High Energy Phys. 07 (2018) 121.

[40] D. Bečirević, I. Doršner, S. Fajfer, N. Košnik, D. A. Faroughy, and O. Sumensari, Scalar leptoquarks from grand unified theories to accommodate the B-physics anomalies, Phys. Rev. D **98**, 055003 (2018).

[41] J. Kumar, D. London, and R. Watanabe, Combined explanations of the $b \to s\mu^+\mu^-$ and $b \to c\tau^-\bar{\nu}$ anomalies: A general model analysis, Phys. Rev. D **99**, 015007 (2019).

[42] Q.-Y. Hu, X.-Q. Li, Y. Muramatsu, and Y.-D. Yang, R-parity violating solutions to the $R_{D^{(*)}}$ anomaly and their GUT-scale unifications, Phys. Rev. D **99**, 015008 (2019).

[43] T. Faber, M. Hudec, M. Malinský, P. Meinzinger, W. Porod, and F. Staub, A unified leptoquark model confronted with lepton non-universality in B-meson decays, Phys. Lett. B **787**, 159 (2018).

[44] J. Heeck and D. Teresi, Pati-Salam explanations of the B-meson anomalies, J. High Energy Phys. 12 (2018) 103.

[45] A. Angelescu, D. Bečirević, D. A. Faroughy, and O. Sumensari, Closing the window on single leptoquark solutions to the B-physics anomalies, J. High Energy Phys. 10 (2018) 183.

[46] S. Bifani, S. Descotes-Genon, A. Romero Vidal, and M.-H. Schune, Review of lepton universality tests in B decays, J. Phys. G **46**, 023001 (2019).

[47] S. Bansal, R. M. Capdevilla, and C. Kolda, Constraining the minimal flavor violating leptoquark explanation of the $R_{D^{(*)}}$ anomaly, Phys. Rev. D **99**, 035047 (2019).

[48] T. Mandal, S. Mitra, and S. Raz, $R_{D^{(*)}}$ motivated $\mathcal{S}_1$ leptoquark scenarios: Impact of interference on the exclusion limits from LHC data, Phys. Rev. D **99**, 055028 (2019).

[49] S. Iguro, T. Kitahara, R. Watanabe, and K. Yamamoto, D^* polarization vs $R_{D^{(*)}}$ anomalies in the leptoquark models, J. High Energy Phys. 02 (2019) 194.

[50] J. Aebischer, A. Crivellin, and C. Greub, QCD improved matching for semi-leptonic B decays with leptoquarks, Phys. Rev. D **99**, 055002 (2019).

[51] S. Bar-Shalom, J. Cohen, A. Soni, and J. Wudka, Phenomenology of TeV-scale scalar Leptoquarks in the EFT, Phys. Rev. D **100**, 055020 (2019).

[52] T. J. Kim, P. Ko, J. Li, J. Park, and P. Wu, Correlation between $R_{D^{(*)}}$ and top quark FCNC decays in leptoquark models, J. High Energy Phys. 07 (2019) 025.

[53] P. Arnan, D. Bečirević, F. Mescia, and O. Sumensari, Probing low energy scalar leptoquarks by the leptonic W and Z couplings, J. High Energy Phys. 02 (2019) 109.

[54] B. Bhattacharya, A. Datta, J.-P. Guévin, D. London, and R. Watanabe, Simultaneous explanation of the R_K and $R_{D^{(*)}}$ puzzles: A model analysis, J. High Energy Phys. 01 (2017) 015.

[55] S. Sahoo and R. Mohanta, Impact of vector leptoquark on $\bar{B} \to \bar{K}^* l^+ l^-$ anomalies, J. Phys. G **45**, 085003 (2018).

[56] A. Crivellin, C. Greub, D. Muller, and F. Saturnino, Importance of Loop Effects in Explaining the Accumulated Evidence for New Physics in B Decays with a Vector Leptoquark, Phys. Rev. Lett. **122**, 011805 (2019).

[57] A. Biswas, D. Kumar Ghosh, N. Ghosh, A. Shaw, and A. K. Swain, Novel collider signature of U_1 Leptoquark and $B \to \pi$ observables, arXiv:1808.04169.

[58] S. Balaji, R. Foot, and M. A. Schmidt, A chiral SU(4) explanation of the $b \to s$ anomalies, Phys. Rev. D **99**, 015029 (2019).

[59] A. Biswas, A. K. Swain, and A. Shaw, Collider signature of V_2 Leptoquark with $b \to s$ flavour observables, Lett. High Energy Phys. **2**, 126 (2019).

[60] J. Roy, Probing leptoquark chirality via top polarization at the colliders, arXiv:1811.12058.

[61] B. Fornal, S. A. Gadam, and B. Grinstein, Left-right SU(4) vector leptoquark model for flavor anomalies, Phys. Rev. D **99**, 055025 (2019).

[62] H. Fritzsch and P. Minkowski, Unified interactions of leptons and hadrons, Ann. Phys. (Leipzig) **93**, 193 (1975).

[63] H. Georgi, The state of the art–gauge theories, AIP Conf. Proc. **23**, 575 (1975).

[64] D. Chang, R. N. Mohapatra, and M. K. Parida, Decoupling Parity and SU(2)-R Breaking Scales: A New Approach to Left-Right Symmetric Models, Phys. Rev. Lett. **52**, 1072 (1984).

[65] D. Chang, R. N. Mohapatra, and M. K. Parida, A new approach to left-right symmetry breaking in unified gauge theories, Phys. Rev. D **30**, 1052 (1984).

[66] D. Chang, R. N. Mohapatra, J. Gipson, R. E. Marshak, and M. K. Parida, Experimental tests of new SO(10) grand unification, Phys. Rev. D **31**, 1718 (1985).

[67] N. G. Deshpande, E. Keith, and P. B. Pal, Implications of LEP results for SO(10) grand unification, Phys. Rev. D **46**, 2261 (1992).

[68] B. Bajc, A. Melfo, G. Senjanovic, and F. Vissani, Yukawa sector in non-supersymmetric renormalizable SO(10), Phys. Rev. D **73**, 055001 (2006).

[69] S. Bertolini, L. Di Luzio, and M. Malinsky, Intermediate mass scales in the non-supersymmetric SO(10) grand unification: A Reappraisal, Phys. Rev. D **80**, 015013 (2009).

[70] K. S. Babu and R. N. Mohapatra, Coupling unification, GUT-scale baryogenesis and neutron-antineutron oscillation in SO(10), Phys. Lett. B **715**, 328 (2012).

[71] G. Altarelli and D. Meloni, A non supersymmetric SO(10) grand unified model for all the physics below M_{GUT}, J. High Energy Phys. 08 (2013) 021.

[72] U. Aydemir, SO(10) grand unification in light of recent LHC searches and colored scalars at the TeV-scale, Int. J. Mod. Phys. A **31**, 1650034 (2016).

[73] U. Aydemir and T. Mandal, LHC probes of TeV-scale scalars in SO(10) grand unification, Adv. High Energy Phys. **2017**, 7498795 (2017).

[74] K. S. Babu and S. Khan, Minimal nonsupersymmetric $SO(10)$ model: Gauge coupling unification, proton decay, and fermion masses, Phys. Rev. D **92**, 075018 (2015).

[75] K. S. Babu, B. Bajc, and S. Saad, Yukawa sector of minimal SO(10) unification, J. High Energy Phys. 02 (2017) 136.

[76] P. Cox, A. Kusenko, O. Sumensari, and T. T. Yanagida, SU(5) unification with TeV-scale leptoquarks, J. High Energy Phys. 03 (2017) 035.

[77] J. C. Pati and A. Salam, Lepton number as the fourth color, Phys. Rev. D **10**, 275 (1974); Erratum, Phys. Rev. D **11**, 703(E) (1975).

[78] G. R. Dvali, Light color triplet Higgs is compatible with proton stability: An Alternative approach to the doublet-triplet splitting problem, Phys. Lett. B **372**, 113 (1996).

[79] A. Maiezza, M. Nemevsek, F. Nesti, and G. Senjanovic, Left-right symmetry at LHC, Phys. Rev. D **82**, 055022 (2010).

[80] P. Bandyopadhyay and R. Mandal, Vacuum stability in an extended standard model with a leptoquark, Phys. Rev. D **95**, 035007 (2017).

[81] D. R. T. Jones, The two loop beta function for a $G(1) \times G(2)$ gauge theory, Phys. Rev. D **25**, 581 (1982).

[82] M. Lindner and M. Weiser, Gauge coupling unification in left-right symmetric models, Phys. Lett. B **383**, 405 (1996).

[83] C. Patrignani *et al.* (Particle Data Group), Review of particle physics, Chin. Phys. C **40**, 100001 (2016).

[84] S. Schael *et al.* (SLD Electroweak Group, DELPHI, ALEPH, SLD, SLD Heavy Flavour Group, OPAL, LEP Electroweak Working Group, L3 Collaborations), Precision electroweak measurements on the Z resonance, Phys. Rep. **427**, 257 (2006).

[85] K. Abe *et al.* (Super-Kamiokande Collaboration), Search for proton decay via $p \to e^+\pi^0$ and $p \to \mu^+\pi^0$ in 0.31 megaton 7 years exposure of the Super-Kamiokande water Cherenkov detector, Phys. Rev. D **95**, 012004 (2017).

[86] P. Langacker, Grand unified theories and proton decay, Phys. Rep. **72**, 185 (1981).

[87] A. M. Sirunyan *et al.* (CMS Collaboration), Search for third-generation scalar leptoquarks decaying to a top quark and a τ lepton at $\sqrt{s} = 13$ TeV, Eur. Phys. J. C **78**, 707 (2018).

[88] A. M. Sirunyan *et al.* (CMS Collaboration), Constraints on models of scalar and vector leptoquarks decaying to a quark and a neutrino at $\sqrt{s} = 13$ TeV, Phys. Rev. D **98**, 032005 (2018).

[89] M. Tanaka and R. Watanabe, New physics in the weak interaction of $\bar{B} \to D^{(*)}\tau\bar{\nu}$, Phys. Rev. D **87**, 034028 (2013).

[90] K. Adamczyk *et al.* (Belle, Belle-II Collaborations), Semitauonic B decays at Belle/Belle II, in *Proceedings of the 10th International Workshop on the CKM Unitarity Triangle (CKM 2018) Heidelberg, Germany, 2018* (Zenodo, 2019), https://arxiv.org/abs/1901.06380.

[91] M. Blanke, A. Crivellin, S. de Boer, T. Kitahara, M. Moscati, U. Nierste, I. Nišandžić, and T. Kitahara, Impact of polarization observables and $B_c \to \tau\nu$ on new physics explanations of the $b \to c\tau\nu$ anomaly, Phys. Rev. D **99**, 075006 (2019).

[92] S. Bhattacharya, S. Nandi, and S. Kumar Patra, $b \to c\tau\nu_\tau$ decays: A catalogue to compare, constrain, and correlate new physics effects, Eur. Phys. J. C **79**, 268 (2019).

[93] J. Grygier *et al.* (Belle Collaboration), Search for $B \to h\nu\bar{\nu}$ decays with semileptonic tagging at Belle, Phys. Rev. D **96**, 091101 (2017); Publisher's Note, Phys. Rev. D**97**, 099902 (2018).

[94] C. Degrande, C. Duhr, B. Fuks, D. Grellscheid, O. Mattelaer, and T. Reiter, UFO—The universal Feynrules output, Comput. Phys. Commun. **183**, 1201 (2012).

[95] J. Alwall, R. Frederix, S. Frixione, V. Hirschi, F. Maltoni, O. Mattelaer, H.-S. Shao, T. Stelzer, P. Torrielli, and M. Zaro, The automated computation of tree-level and next-to-leading order differential cross sections, and their matching to parton shower simulations, J. High Energy Phys. 07 (2014) 079.

[96] R. D. Ball *et al.*, Parton distributions with LHC data, Nucl. Phys. **B867**, 244 (2013).

[97] T. Mandal, S. Mitra, and S. Seth, Pair production of scalar leptoquarks at the LHC to NLO parton shower accuracy, Phys. Rev. D **93**, 035018 (2016).

[98] T. Mandal and S. Mitra, Probing color octet electrons at the LHC, Phys. Rev. D **87**, 095008 (2013).

[99] T. Mandal, S. Mitra, and S. Seth, Single productions of colored particles at the LHC: An example with scalar leptoquarks, J. High Energy Phys. 07 (2015) 028.

[100] T. Mandal, S. Mitra, and S. Seth, Probing compositeness with the CMS $eejj$ & eej data, Phys. Lett. B **758**, 219 (2016).

[101] S. Bansal, R. M. Capdevilla, A. Delgado, C. Kolda, A. Martin, and N. Raj, Hunting leptoquarks in monolepton searches, Phys. Rev. D **98**, 015037 (2018).

[102] M. Aaboud *et al.* (ATLAS Collaboration), Search for additional heavy neutral Higgs and gauge bosons in the ditau final state produced in 36 fb^{-1} of pp collisions at $\sqrt{s} = 13$ TeV with the ATLAS detector, J. High Energy Phys. 01 (2018) 055.

[103] M. Aaboud *et al.* (ATLAS Collaboration), Search for High-Mass Resonances Decaying to $\tau\nu$ in pp Collisions at $\sqrt{s} = 13$ TeV with the ATLAS Detector, Phys. Rev. Lett. **120**, 161802 (2018).

[104] K. Chandak, T. Mandal, and S. Mitra, Hunting for scalar leptoquarks with boosted tops and light leptons, Phys. Rev. D **100**, 075019 (2019).

[105] M. E. Machacek and M. T. Vaughn, Two loop renormalization group equations in a general quantum field theory. 2. Yukawa couplings, Nucl. Phys. **B236**, 221 (1984).

[106] F. Staub, SARAH 3.2: Dirac Gauginos, UFO output, and more, Comput. Phys. Commun. **184**, 1792 (2013).